CIAMTIS

U.S. DOT Region 3 University Transportation Center

Life Extension of Fatigue-Damaged Highway, Rail, and Transit Bridges

May 1, 2021

Prepared by:

Alexandra Tracy, Richard Sause, Ian Hodgson, and Joe Saunders

Lehigh University

r3utc.psu.edu

PennState College of Engineering

LARSON TRANSPORTATION INSTITUTE

DISCLAIMER

The contents of this report reflect the views of the authors, who are responsible for the facts and the accuracy of the information presented herein. This document is disseminated in the interest of information exchange. The report is funded, partially or entirely, by a grant from the U.S. Department of Transportation's University Transportation Centers Program. However, the U.S. Government assumes no liability for the contents or use thereof.

Technical Report Documentation Page

1. Report No.	2. Government Accession No.	3. Recipient's Catalog No.
CIAM-UTC-REG 8		

4. Title and Subtitle	5. Report Date
Life Extension of Fatigue-Damaged Highway, Rail, and Transit Bridges	May 1, 2021
	6. Performing Organization Code

7. Author(s)	8. Performing Organization Report No.
Alexandra Tracy, Richard Sause, Ian Hodgson, and Joe Saunders	

9. Performing Organization Name and Address	10. Work Unit No. (TRAIS)
Lehigh University ATLSS Engineering Research Center 117 ATLSS Drive Bethlehem, PA 18015	11. Contract or Grant No. 69A3551847103

12. Sponsoring Agency Name and Address	13. Type of Report and Period Covered
U.S. Department of Transportation Research and Innovative Technology Administration 3rd Fl, East Bldg E33-461 1200 New Jersey Ave, SE Washington, DC 20590	Final Report 3-1-2019-3-31-2020
	14. Sponsoring Agency Code

15. Supplementary Notes

Work funded through The Pennsylvania State University through the University Transportation Center Grant Agreement, Grant No. 69A3551847103.

16. Abstract

Fatigue is a common and potentially very damaging occurrence in metallic structures, including steel bridges. There have been numerous studies throughout the last two centuries on fatigue life, but challenges of preventing fatigue crack growth are still unresolved. The most widespread method of repair and retrofitting involves drilling a crack-arrest hole at the tip of a fatigue crack, but crack re-initiation has been noted in many cases of this repair. The purpose of this study was to better understand re-initiation at crack-arrest holes through welds and to develop methods to prevent re-initiation from occurring.

17. Key Words	18. Distribution Statement
Fatigue cracking, steel bridge, stress, crack-arrest hole	No restrictions. This document is available from the National Technical Information Service, Springfield, VA 22161

19. Security Classif. (of this report)	20. Security Classif. (of this page)	21. No. of Pages	22. Price
Unclassified	Unclassified	155	

TABLE OF CONTENTS

Reports included in Appendix:

Fatigue Life Estimation of Bridges with Smart Mobile Sensing (Helen Whalen)

Efficient Service Life Extension of Bridges Through Risk-Based Life-Cycle Management and High-Performance Construction Materials: Emphasis on Corrosion-Resistant Steel (Tristan Golden)

Road Pavement Condition Monitoring by Embedded Crowdsensing (Charles Inwald)

LIST OF FIGURES

LIST OF TABLES

Abstract

Fatigue is a common and potentially very damaging occurrence in metallic structures, including steel bridges. There have been numerous studies throughout the last two centuries on fatigue life, but challenges of preventing fatigue crack growth are still unresolved. The most widespread method of repair and retrofitting involves drilling a crack-arrest hole at the tip of a fatigue crack, but crack re-initiation has been noted in many cases of this repair. The purpose of this study is to better understand re-initiation at crack-arrest holes through welds and to develop methods to prevent re-initiation from occurring.

1. Introduction

1.1 Historical Background

Some of the first fatigue-related issues were recorded in structures starting in the 19th century with the introduction of the industrial era. German and British engineers performed laboratory fatigue tests with cyclic stresses subjected to bending, torsion and axial loads[3]. The growing use of iron and steel in manufacturing, industrial, and transportation industries led to some reports of fatigue or fracture failures in elements such as mine hoists, railroad bridge members, railroad car axles, pressure vessels, and storage tanks[3]. However, up until the early 1960s, fatigue and fracture design was not typically considered.

During the AASHO Road Test in 1960, fatigue cracks were observed in cover-plated steel bridge beams due to heavy loads and large stress ranges[3]. This project inspired experimental studies supported by the National Cooperative Highway Research Program, including Project 12-7 which was carried out at Fritz Laboratory, Lehigh University in 1967. These studies revealed that the most significant factors for evaluating fatigue strength are the stress range and the type of detail. For different structural details, fatigue cracking initiated at

discontinuities in the weld or base metal, and was highly correlated with the applied stress range[2]. These findings were applicable to rolled beams, welded beams, beams with groove-welded flange splices, coverplated beams, and beams with welded stiffeners and attachments[2]. Specifications related to this research were developed and implemented in the AASHTO *Standard Specifications for Highway Bridges*, but fatigue-related issues still occurred in structures.

1.2 Importance of Fatigue Research

Fatigue strength is important to consider because a repeated loading of structural components can lead to fatigue cracking or failure. Although fatigue is a common and potentially critical form of structural damage, how and why re-initiation occurs at crack-arrest holes through welds is not fully understood.

Currently, S-N curves are customarily used to evaluate fatigue life, as they relate the stress range of a material or detail to the number of cycles to failure. These curves were first developed in 1842 by German scientist August Wöhler, who discovered that after fatigue cracks reach a critical size, they will quickly propagate to failure[5]. However, it was not until 1974 that the AASHTO *Standard Specifications for Highway Bridges* began to use fatigue design concepts. Six fatigue categories, A through F, were added to the AASHTO specifications in order to provide the fatigue resistance for different types of details[5]. In the following years, welding procedures were more strictly defined, as defects in welding can cause a detail to be prone to fatigue cracking.

The specifications surrounding fatigue design in the AASHTO are still fairly minimal. The main points of concern are: determining the number of cycles which the detail is subjected to, identifying the Detail Category for each component of the structure, calculating the

permissible stress ranges for the components of a structure that are sensitive to fatigue and comparing those results with the actual stress ranges[1].

While the fatigue code for bridges has increased the fatigue life in newer bridges, many older bridges need to be evaluated or repaired due to fatigue issues. A current method for stopping crack growth include identifying the geometry a fatigue crack, then drilling a crack-arrest hole with a diameter that satisfies the following equation:

$$D = \frac{S_r \pi a}{8\sigma_y} \geq 1.0\ in.$$

S_r = nominal stress range where the crack tip is located

a = half the crack length (in)

σ_y = yield stress of the material (ksi)

This equation is specific for crack-arrest holes for distortion induced cracking.

1.3 Research Approach

There are three different phases of analysis and laboratory testing to assess the fatigue resistance of re-initiation of crack-arrest hole through welds. Phase 1 will validate and assess crack re-initiation at crack-arrest holes. A steel plate specimen with a crack-like opening and two crack-arrest holes on either end of the opening will be cyclically loaded until re-initiation occurs. This phase of testing will consider the effect the crack-arrest hole diameter and the applied stress range has on the fatigue resistance. Phase 2 will analyze and test a steel fillet welded tee-joint, and confirm weld toe cracking is consistent with AASHTO Fatigue Category C. Phase 3 will be a combination of the first two experiments. Analysis and laboratory testing of a steel fillet welded tee-joint with a crack-like opening along the weld toe, and crack-arrest holes will be performed. Each phase of laboratory testing will be performed on an MTS-810 servohydraulic

computer-controlled universal material testing machine in ATLSS Engineering Center, Lehigh University.

1.4 Objectives & Scope

Fatigue cracking is one of the primary forms of damage that a steel bridge experiences. Fatigue cracking occurs after a structure has undergone cyclic stressing or loading, such as traffic loading. However, with consideration of fatigue specifications, fatigue cracks are not a significant concern for most modern bridges. Nonetheless, if allowed to grow, fatigue cracks can lead to very expensive repairs and sometimes failure of a bridge. Older bridges were not built with the same knowledge of fatigue, and since repair and retrofit methods have been used, however, these methods have not always prevented re-initiation. This project will broaden knowledge how fatigue cracks re-initiate at retrofit holes and develop our understanding and methods to prevent re-initiation from occurring.

2. Development of Design

2.1 Phase 1 - Plate with Two Crack-Arrest Holes and Crack-Like Opening

Finite element models, created in the program Abaqus CAE, were used to determine the design and dimensions of the steel specimen. In order to understand crack re-initiation, a steel plate model was designed, consisting of a ½" thick plate with two holes arresting each end of a single crack-like opening. In order to produce fatigue cracking at the outer edge of the holes, the model must have a net stress and gross stress high enough to re-initiate cracking, yet not have a max stress higher than yield in order to ensure linear-elastic behavior. Knowing what the target stresses are, the geometry was altered until a suitable design was created.

Additionally, a mesh convergence study of the design was performed to ensure the accuracy of the analysis. Meshes of 1/2", 1/10", and 1/20" were taken into consideration (See

Appendix 2-4). To visualize this data, a graph was produced by plotting mesh size against maximum principal stress, which occurred at the outer portion of both crack-arrest holes on the model (See Appendix 5). Due to the computational effort to run the models with the finer mesh sizes and the convergence of stress, a 1/10" was selected as an effective mesh size.

To validate the resulting stresses from the finite element analysis (FEA), theoretical calculations were performed and then compared to the simulated results. Given the geometry and the fact that the stress concentration for two holes connected by a slit under tension is equivalent to an ellipse (see Appendix 6 for further explanation), the following equation was used to calculate the stress concentration:

$$K_{tn} = C_1 + C_2(2a/H) + C_3(2a/H)^2 + C_4(2a/H)^3$$

where the C values are derived from the following table (See Appendix 7 for more details).

	$1.0 \leqslant a/b \leqslant 8.0$
C_1	$1.109 - 0.188\sqrt{(a/b)} + 2.086(a/b)$
C_2	$-0.486 + 0.213\sqrt{(a/b)} - 2.588(a/b)$
C_3	$3.816 - 5.510\sqrt{(a/b)} + 4.638(a/b)$
C_4	$-2.438 + 5.485\sqrt{(a/b)} - 4.126(a/b)$

After the FEA results had been verified with the theoretical calculations, three more models of plates with two crack-arrest holes and a crack-like opening were designed. These other models included variations in the two variables taken into consideration, the stress range and the arrest-hole diameter. The FEA results for these designs were also verified with the theoretical calculations. The results for the FEA are shown in Table 1.

2.2 Final Designs for Phase 1

The specimen design that will be tested is a 12" x 24" x ½" plate with a crack-like opening in-between two crack-arrest holes. In order to gain thorough data, there will be two

variables taken into consideration: the diameters for the holes and the applied stress range. This will result in eight different experiments: two specimens with target net stress ranges of approximately 18 ksi, one with 2.5 inch diameter crack-arrest holes and one with 3 inch diameter crack-arrest holes and two specimens with target net stress ranges of approximately 22 ksi, one with 2.5 inch diameter crack-arrest holes and one with 3 inch diameter crack-arrest holes.

Table 1. FEA Data for Final Designs

Model	Seam (in)	Hole Diameter (in)	Edge Length (in)	Load (kips)	Gross Stress (ksi)	Net Stress (ksi)	Hole Stress (ksi)	SCFg	SCFn
H12_Holes3_Seam2_Load36	2	3	3.5	36	6.00	18.5899	45.6571	7.615	2.456
H12_Holes5_2_Seam3_Load36	3	2.5	3.25	36	6.01	18.3909	47.6846	7.936	2.593
H12_Holes3_Seam2_Load44	2	3	3.5	44	7.33	22.7209	55.8031	7.615	2.456
H12_Holes5_2_Seam3_Load44	3	2.5	3.25	44	7.34	22.4778	58.2812	7.936	2.593

Table 2. Theoretical Hole Stress

Model	Seam (in)	Hole Diameter (in)	Edge Length (in)	Load (kips)	Gross Stress (ksi)	Net Stress (ksi)	Hole Stress (ksi)	SCFg	SCFn
H12_Holes3_Seam2_Load36	2	3	3.5	36	6	18	46.91	7.82	2.61

H12_Holes5_2_Seam3_Load36	3	2.5	3.25	36	6	18	49.34	8.22	2.74
H12_Holes3_Seam2_Load44	2	3	3.5	44	7.33	22	57.33	7.82	2.61
H12_Holes5_2_Seam3_Load44	3	2.5	3.25	44	7.33	22	60.30	8.22	2.74

3 Preliminary Results

Before running laboratory tests with the designed speimens, a preliminary test was performed. The specimen tested was 12” x 24” x 3/8” with crack-arrest holes of 2.5 inch diameters and a 3 inch crack-like opening connecting the two holes. The specimen was loaded cyclically from 4 kips to 40 kips, providing a load range of 36 kips. Strain gauges were attached to both sides of the plate, 6 inches from either end of the plate, and on the inside of both arrest-holes (See Appendix 8). This test was not run until re-initiation due to unexpected problems with the testing equipment, however, the test will be completed in the near future. Below are the results from the cyclical loading output (Figure 1) and from readings on strain gauges 5 and 6. There is a slight lapse in time between the output of the loading commands and the stress results, as seen by comparing the graphs.

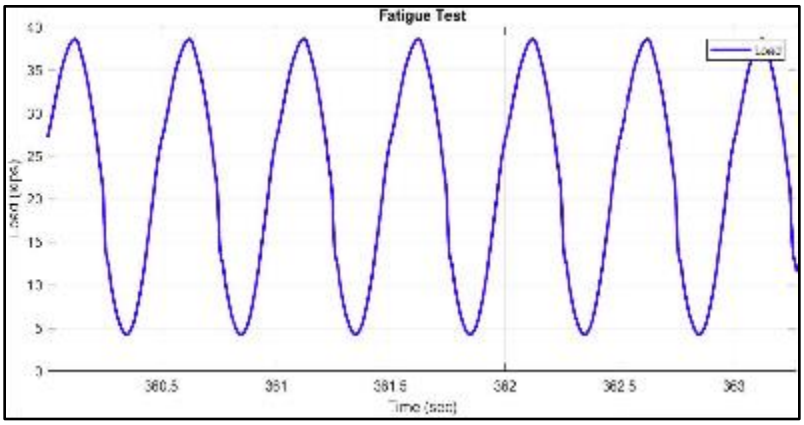

Figure 1. Preliminary Fatigue Test Results (Load vs. Time)

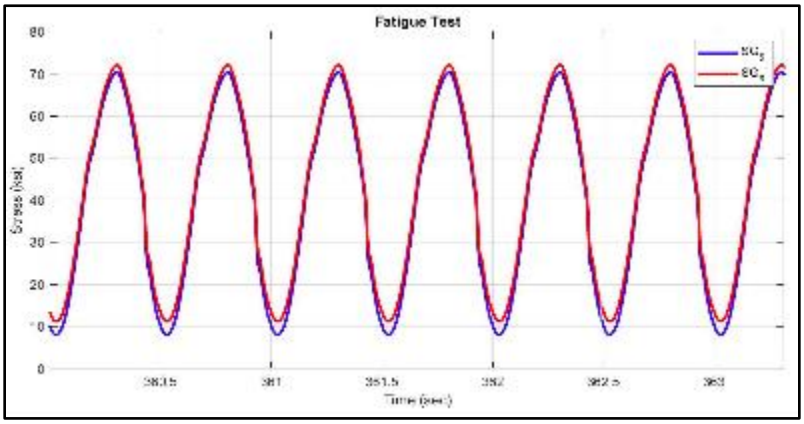

Figure 2. Preliminary Fatigue Test Results (Stress at the Crack-Arrest Holes vs. Time)

4. Discussion / Further Research

Although there is not enough data to provide any conclusionsfinishing testing of all 8 specimens and the next two phases of the project will provide more insight into how re-initiation occurs. FEA models for the second phase of the project have been modeled, but extensive analysis of that data has not occurred and is included for information purposes. (See Appendix 9-10).

References

1. Fisher, J. W., Kulak, G. L. and Smith, I. F. C. A Fatigue Primer for Structural Engineers. National Steel Bridge Alliance (NSBA), 1998.
2. Fisher, J. W. and Yen, B. T., Fatigue Strength of Steel Members with Welded Details. American Institute Of Steel Construction, 1977.
3. National Research Council (U.S.)., & American Association of State Highway Officials. (1962). The AASHO road test: Report 7: Summary report. Washington: National Academy of Sciences-National Research Council.

4. Isida, M., 1953, On the tension of the strip with semi-circular notches, Trans. Jpn. Soc. Mech. Eng., Vol. 19, p. 5.
5. X. W. Ye, Y. H. Su, and J. P. Han, "A State-of-the-Art Review on Fatigue Life Assessment of Steel Bridges," Mathematical Problems in Engineering, vol. 2014, Article ID 956473, 13 pages, 2014. https://doi.org/10.1155/2014/956473.

Appendix

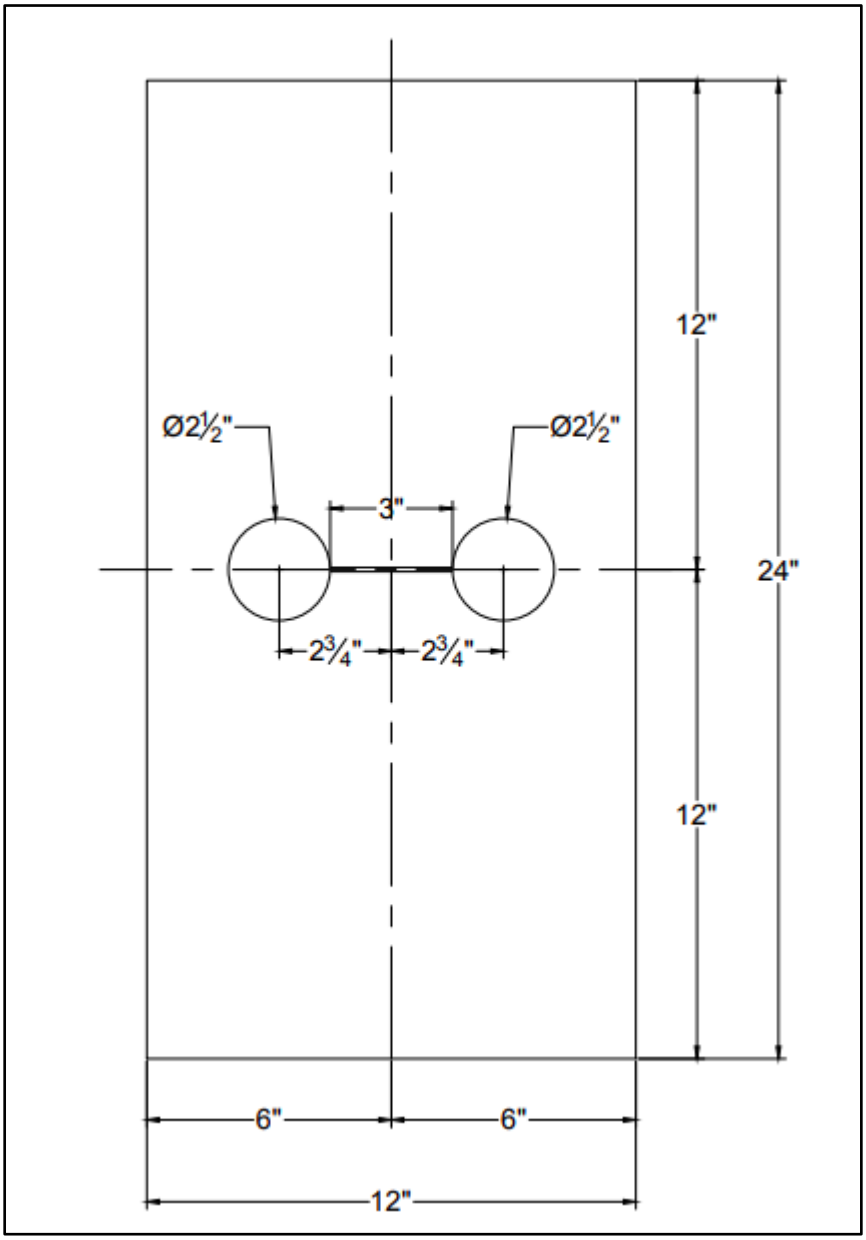

Appendix 1.

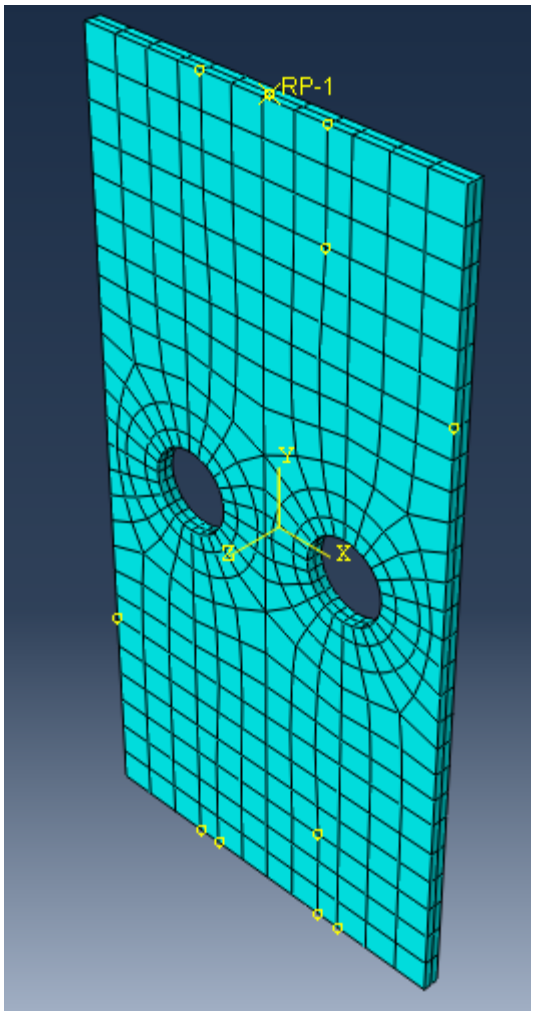

Appendix 2.
FEM with Mesh ½”

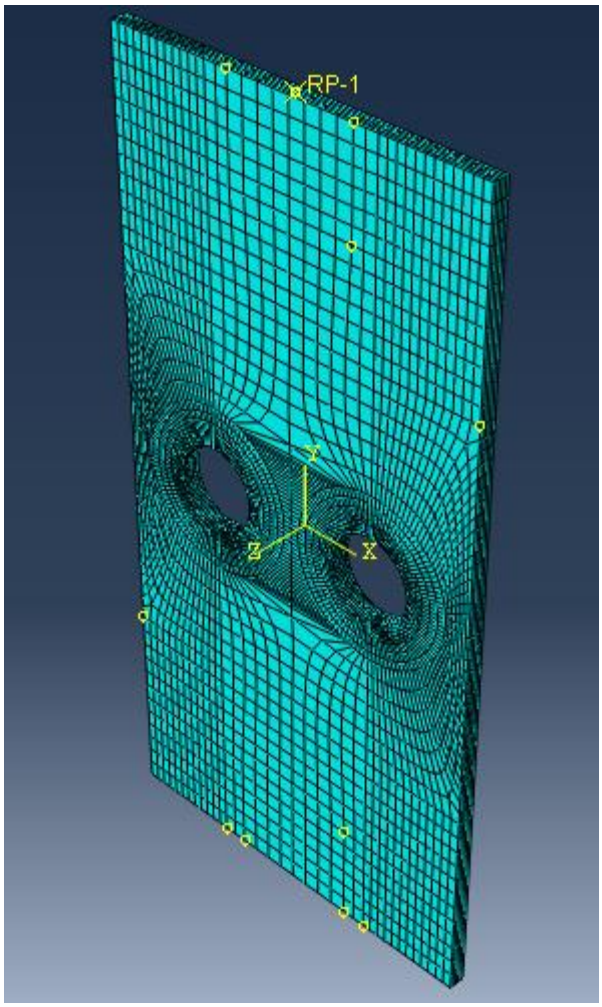

Appendix 3.
FEM with Mesh 1/10”

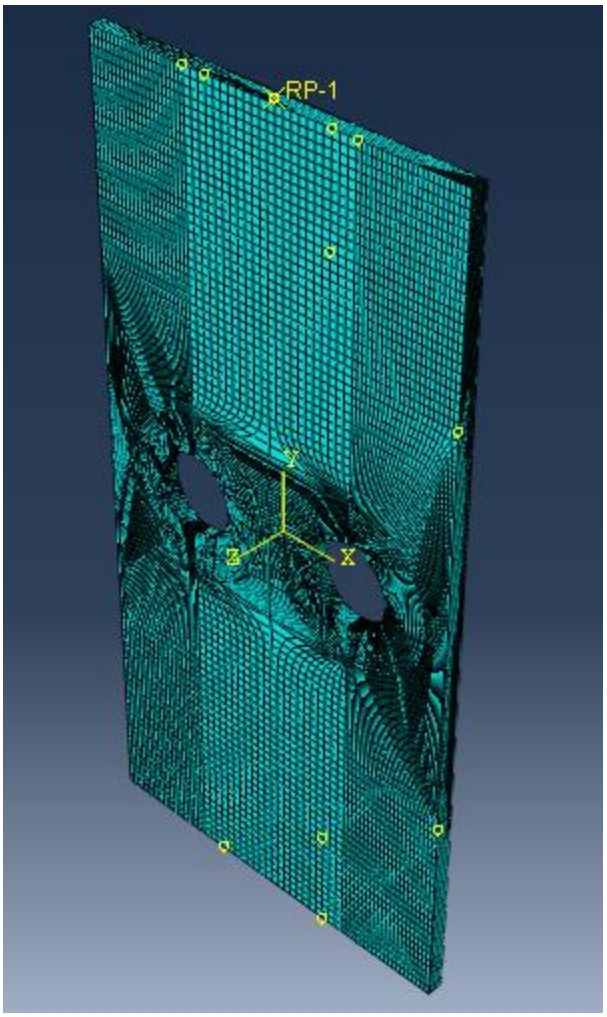

Appendix 4.
FEM with Mesh 1/20”

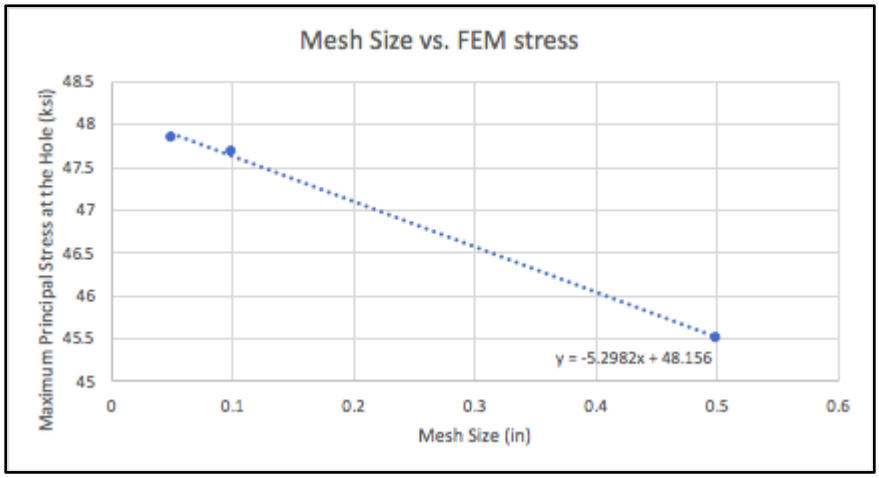

Appendix 5.
Mesh Convergence Study Results

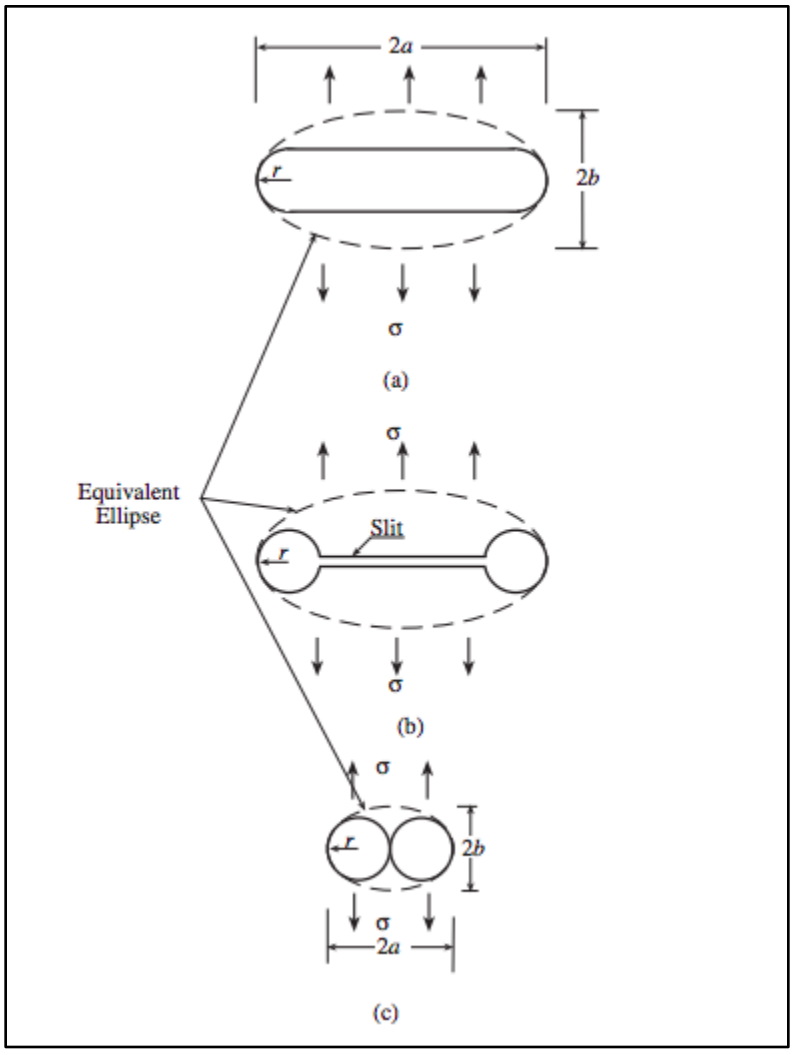

Appendix 6.

Equivalent ellipses: a) ovaloid; b) two holes connected by a slit; c) two tangential circular holes.

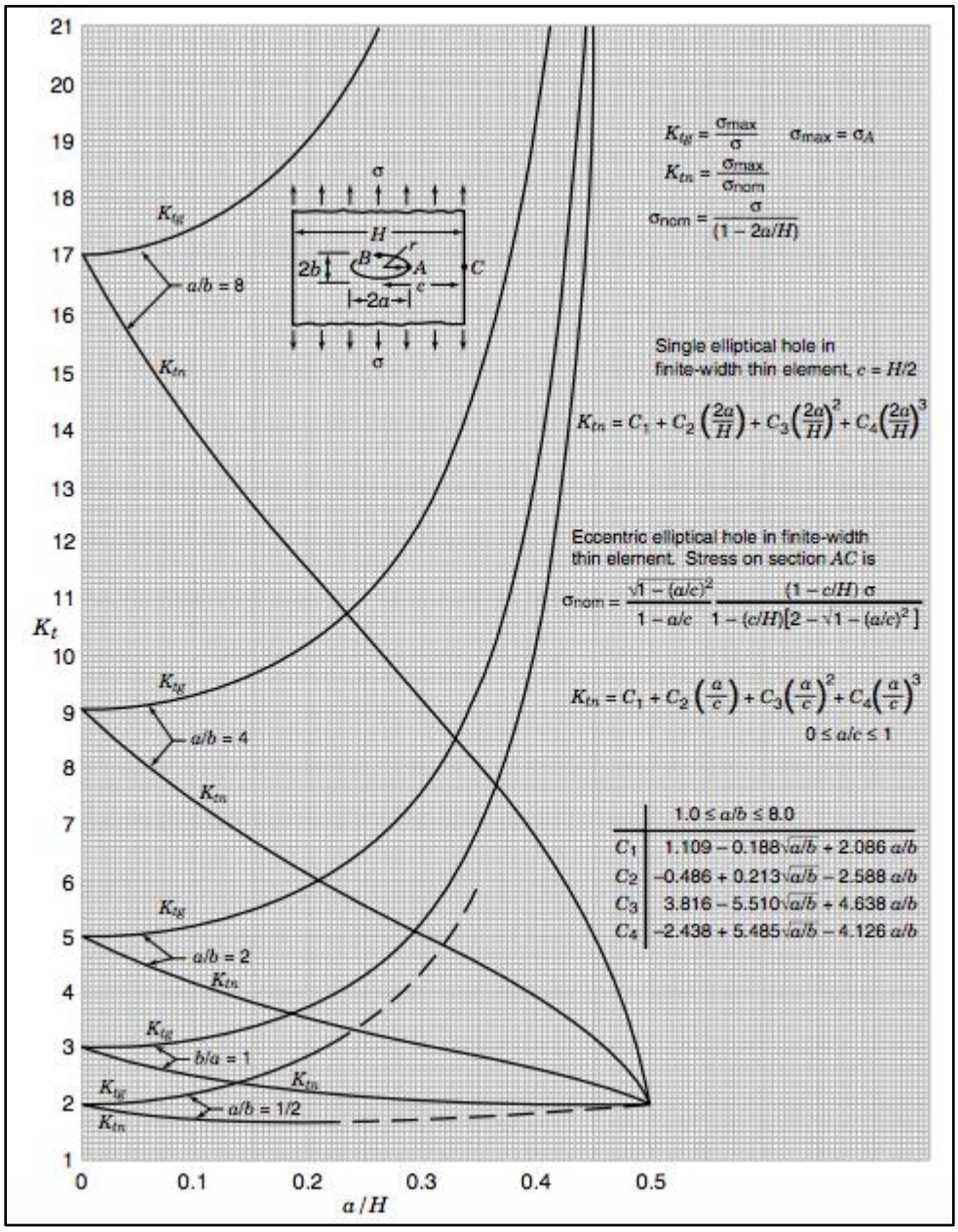

Appendix 7.

Stress concentration factors Ktg and Ktn of an elliptical hole in a finite-width thin element in uniaxial tension

Appendix 8.
Preliminary Test on Specimen Using MTS-810 Machine

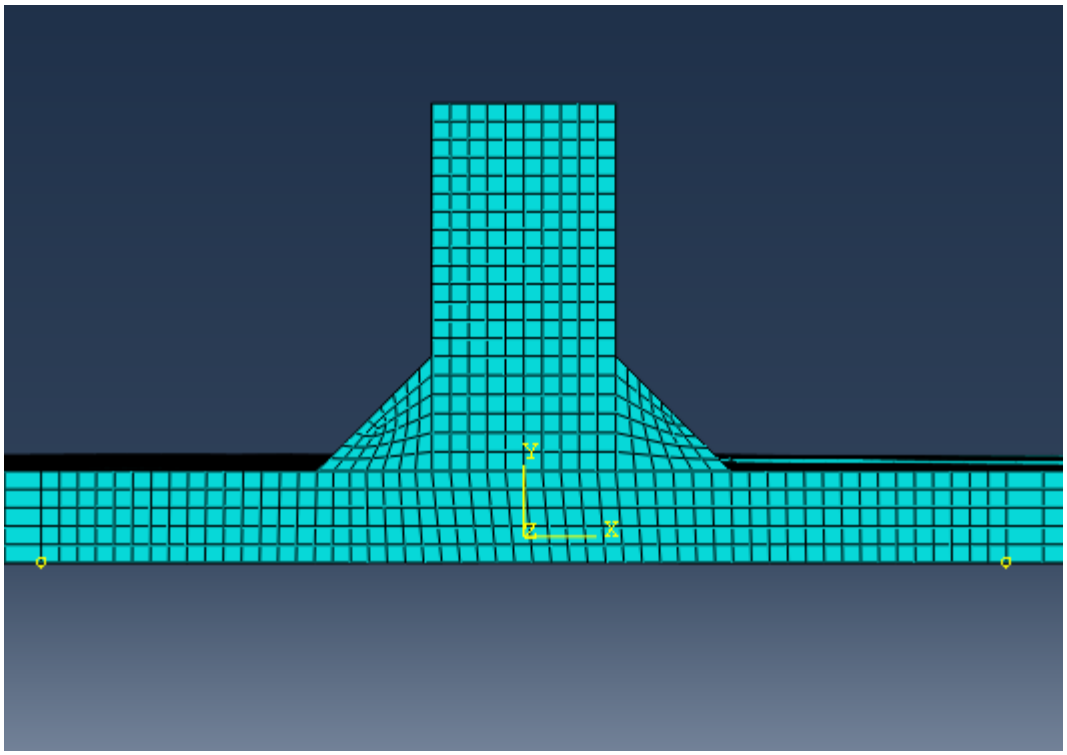

Appendix 9.
Finite Element Model for Fillet Welded Tee-Joint

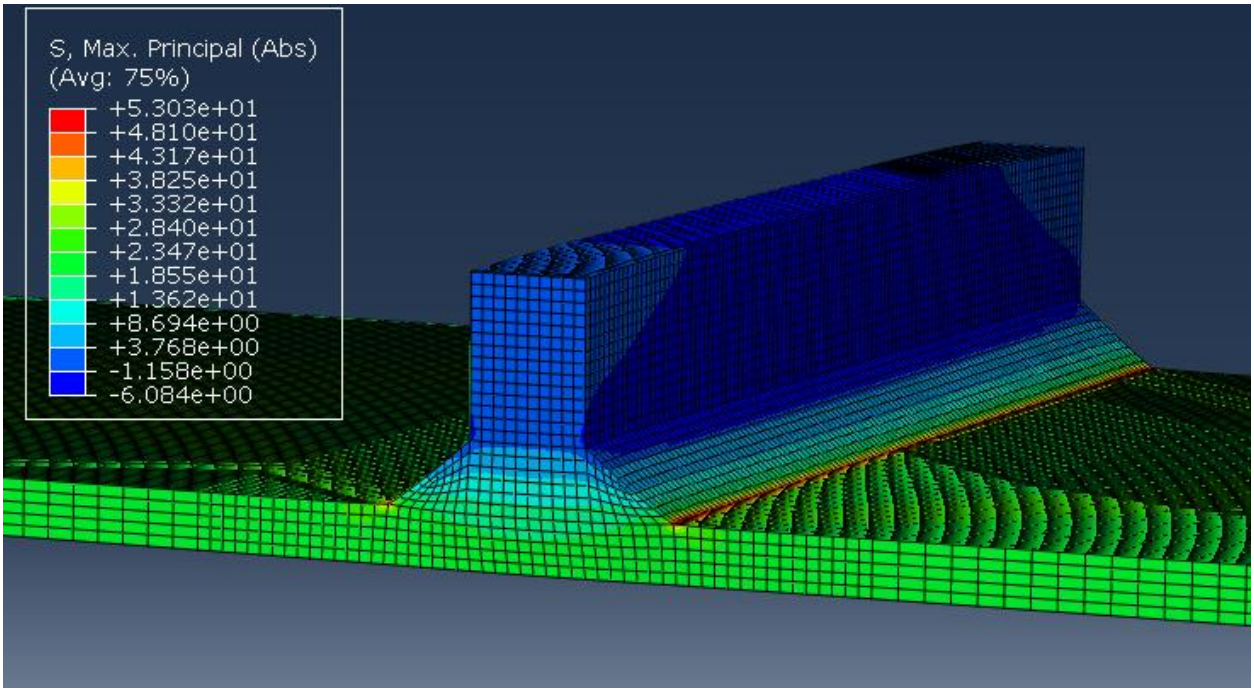

Appendix 10.
Finite Element Model for Fillet Welded Tee-Joint with Stress Analysis Displayed

Fatigue Life Estimation of Bridges with Smart Mobile Sensing

Helen Whalen

Center for Integrated Asset Management for Multi-modal Transportation Infrastructure Systems (CIAMTIS): Region 3 University Transportation Center

ATLSS REU Program
Department of Civil and Environmental Engineering
Lehigh University

Abstract

Civil structures experience significant vibrations and repeated stress cycles during their service life. These conditions are the bases for fatigue analysis to estimate the remaining fatigue life of the structure, which requires a full-field strain assessment over a typical loading period. These strain measurements are traditionally obtained by means of wired strain gauges, which is a quite expensive and laborious procedure as more spatial information is desired. This project aims to estimate the remaining fatigue life of structures by using a deep learning based approach to convert acceleration data into strain data. The proposed methodology utilizes acceleration data collected by means of mobile sensing as inputs to a deep neural network that estimates strain responses. To evaluate the proposed method, a laboratory-scale curved bridge girder subjected to various dynamic loading types is tested. A finite element model of this girder is also created and a modal frequency analysis is conducted to compare with experimental results.

Table of Contents

List of Figures

List of Tables

1. Introduction

Civil structures, specifically bridges, experience significant vibrations and repeated stress cycles during their life periods. Wind, traffic, and thermal loadings, among others cause repeated dynamic loadings in these structures, potentially leading to fatigue failures. Since fatigue is a localized and progressive type of failure, it requires inspection over the structure's service life to determine the remaining fatigue life of that structure. The remaining fatigue life is represented by the number of stress cycles before the fatigue failure. The rainflow counting algorithm is a popular technique that reduces a complex spectrum of varying stress into a set of simple stress reversals to assess the fatigue of a structure subjected to dynamic loading (Downing and Socie). In order to perform this procedure, a full-field strain assessment of the structure over a typical loading period is required. For fatigue analysis, strain measurements are typically obtained using strain gauges. However, large scale deployment of wired strain gauges is expensive and laborious. Using wired strain gauges along the span of a bridge is also impractical; more spatial information is desired as these sensors can be placed only at fixed locations along the member (Kim et al.). These limitations associated with strain gauges call for an innovative sensing strategy in which information can be integrated from an inexpensive data source.

Structural Health Monitoring (SHM) applications often rely on acceleration data, which can be collected relatively inexpensively through mobile sensing. Mobile sensing is becoming a popular area of interest in many fields of engineering. As a type of crowdsensing, mobile sensing allows members of the public to take an active role in data collection, providing more up-to-date information on the structure's health (Matarazzo and Pakzad). Collecting acceleration data by means of mobile sensing also eliminates the spatially-restrictive nature of fixed sensors as a continuous set of data can be collected along a bridge span.

2. Background

With complex structures, it is not possible to perfectly model all aspects of a system; therefore, data-driven approaches have become an attractive alternative for SHM applications. Data-driven approaches substitute a real model with a surrogate model, constructed using acquired data from a system (Sen and Nagarajaiah). Today's advanced technology enables crowdsourcing, leading to an abundance of data. All of this data provides an opportunity to extract information about the condition of infrastructure at an unprecedented rate and resolution. The downside of this abundance of data is a big data problem in storage and analysis. Fatigue life estimation could include years' worth of collected data, making it difficult to store and analyze this amount of data.

Deep learning, or deep neural network (DNN), is an ideal set of techniques used to address the big data problem and exploit the opportunities within big data (Gulgec et al.). DNN algorithms are designed to learn from data, so their performance improves with more data. Figure 1 below depicts the architecture of a deep network.

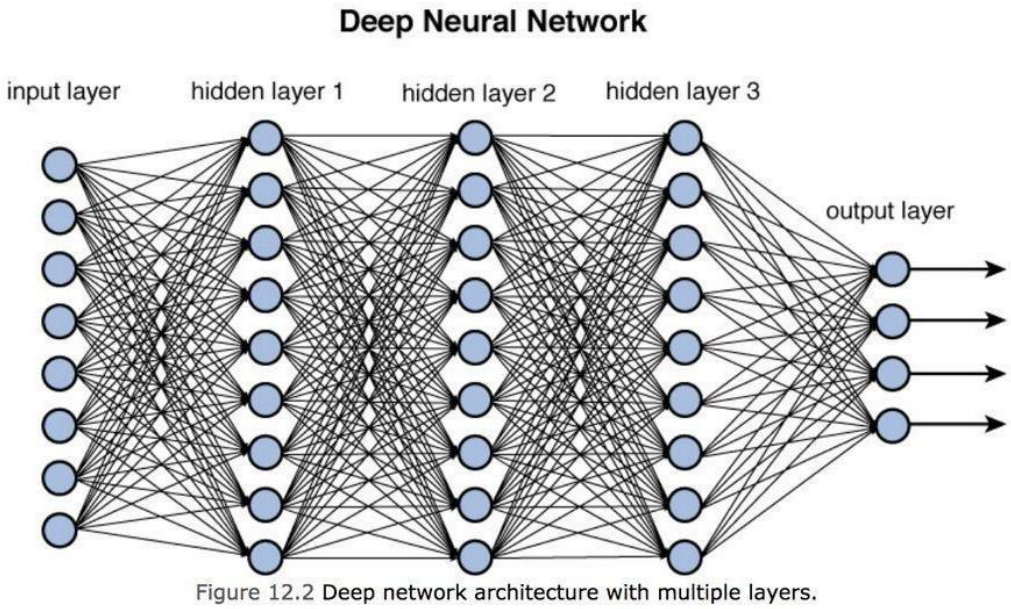

Figure 1: DNN architecture

As illustrated by this figure, DNNs consist of multiple layers that process the input features, and each layer typically extracts some piece of valuable information. During the learning process, the DNN builds a model from the layers that is then used to make data-driven predictions.

For civil engineering applications, dense sensor networks produce dynamic, nonlinear, and spatio-temporal data unique to each structure. Unlike applications in other fields, the collected data provides physical and dynamical information on a structures' properties, condition, and performance. This application requires a customized neural network that exploits the big data while also considering the knowledge of physical characteristics of the system to take advantage of the governing modeling techniques' improved performance.

3. Methodology

3.1 Overview

The goal of this project is to develop a SHM-specialized deep learning framework to find the remaining fatigue life of a structure. This process involves using easily and inexpensively generated structural response data into more expensive measurement estimates. In the case of this study, acceleration data collected by means of mobile sensing will be converted to strain data to estimate the remaining fatigue life of the structure. Figure 2 below shows a general map of the proposed methodology. As depicted in this figure, the data collection process involves using mobile sensing to collect acceleration responses. These mobile sensors simultaneously measure vibration data in time while scanning over a large set of points in space, creating a problematic data arrangement with spatial discontinuities. Therefore, the data conversion phase will convert the collected mobile data to regular acceleration time histories. This converted acceleration data is then used to train the SHM-specialized DNN architecture which incorporates fundamental knowledge from structural analysis and dynamics. The output of this DNN will be estimated

rainflow counting histograms of strain which will be used to estimate the fatigue life of the structure.

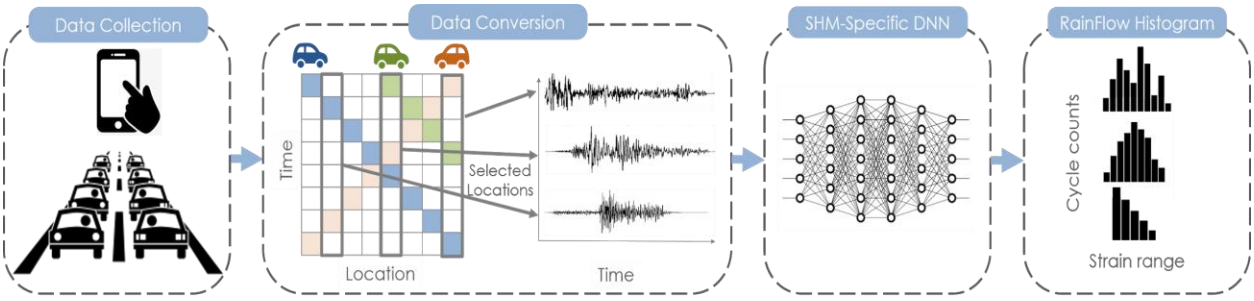

Figure 2: Framework of the proposed methodology

3.2 Experimental Setup

A preliminary study is conducted on a horizontally curved tubular flange girder (TFG) instrumented with six accelerometers (A1 – A6) and four strain gauges (SG1 – SG4) along the span, as shown below in Figure 3. This test specimen is used to evaluate the performance of the proposed methodology on complex geometry.

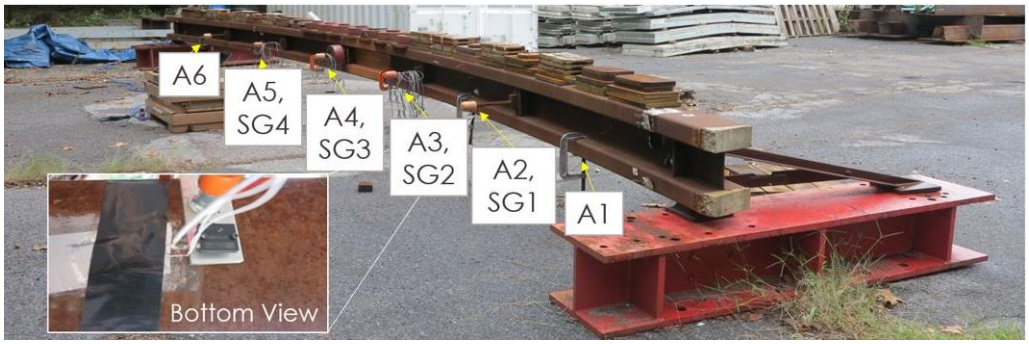

Figure 3: Experimental setup of TFG

Vibration and strain measurements of the curved girder are collected in order to establish the dynamic characteristics of the structure. The distributed weights added to the structure are such that the three lowest mode frequencies are between 5 and 50 Hz. Over the course of two months on various days, four different types of loading were applied to the girder to represent the different types of vibration a bridge may experience during its operation. With the collected vibration data, structural modal analyses were performed to determine the mode shapes and

corresponding frequencies. Using the software package SMIT, modal parameter identification was performed using the output-only Eigensystem Realization Algorithm (ERA), which creates a stabilization diagram that allows one to identify the frequencies at which mode shapes are present (Chang and Pakzad).

3.3 Finite Element Model

A finite element model (FEM) of the girder described in the previous section was created in Abaqus and will be used in the future to obtain vibration response data to be used in the DNN algorithms. At this stage in the project, modal analyses have been performed on this model to obtain the frequencies for the first ten eigenvalues of this girder. These frequencies can be compared to the experimental frequencies obtained using the test specimen, which will be discussed later in the preliminary results section. An image of the model in Abaqus is shown below in Figure 4.

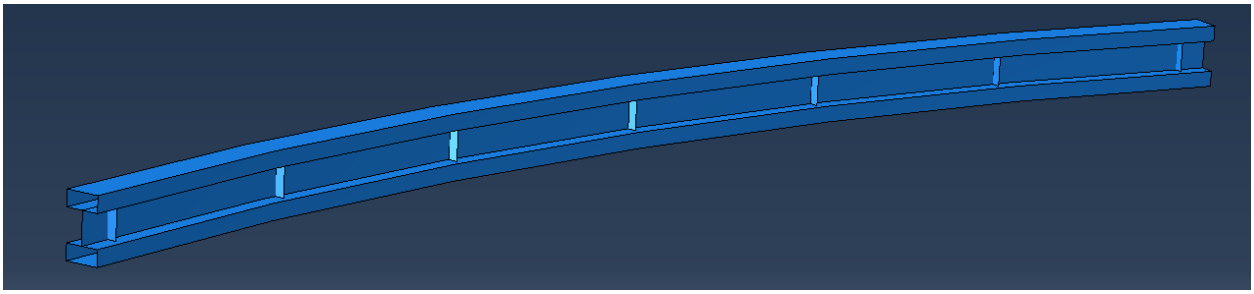

Figure 4: Model of curved girder

This girder was modeled following a similar procedure as a previous study conducted by Eric Putnam in 2010 in which a finite element model of this test specimen was used to analyze the behavior of curved TFGs under vertical load (Putnam). Due to the complex curved geometry of this girder, the parts were first drawn in AutoCAD and then imported into Abaqus. The parts were modeled using homogeneous shell elements with their respective thicknesses assigned. The element type used was the S4 linear 4-node double curved general-purpose shell element. For the material properties of each part, an elastic isotropic steel was assigned with an elastic modulus of

29,000 ksi and a Poisson's ratio of 0.3. To produce accurate results, a fine mesh was chosen with an approximate global size of 0.5". This mesh was assigned to all parts of the girder. The full girder with the mesh assigned can be seen below in Figure 5.

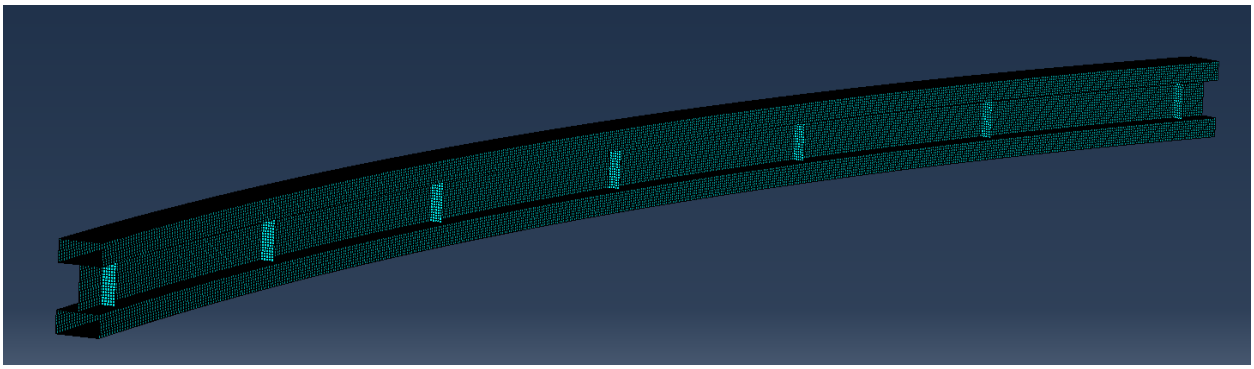

Figure 5: Mesh assigned to TFG

The boundary conditions assigned to this member were modeled to represent the actual conditions on the test specimen. The real test girder is supported by resting on two support beams at 9 inches in from each end. It also has end overturning brackets at each bearing region to prevent cross-section rotation and twisting. In Abaqus, these end conditions were modeled to represent simple supports at the bearing locations. Along the bottom wall of the bottom tube at the centerline of the bearings, the vertical (U3) and radial (U2) displacements were set to zero at both ends. At just the north end, the lateral displacement (U1) was set to zero at the center node along the bearing centerline. To provide the rotational restraint that the end overturning brackets provide, the rotation about the x-axis (UR1) was set to zero at mid depth of the cross section at each bearing location. The boundary conditions at the bearings are shown below in Figure 6.

Figure 6: Boundary conditions on TFG model

The loading applied to this girder was also taken from the previous study conducted by Putnam. A total load of 2560 lbs. was applied as a pressure load on the top flange. This load was

divided by area of the top surface of the top flange to obtain a pressure load across the entire top surface. This loading represents the self-weight of the girder plus an additional distributed load, as was modeled in the actual experiment.

4. Preliminary Results and Discussion

In order to ensure the finite element model is working and models the girder correctly, a linear perturbation frequency analysis step was set up in the Abaqus model. This analysis performs eigenvalue extraction to calculate the natural frequencies and corresponding mode shapes of the system. For this model, the first ten eigenvalues and corresponding frequencies were extracted to try to match some of the values with the experimental frequencies obtained using the software SMIT. The ERA analysis procedure in SMIT previously mentioned outputs a stabilization diagram that shows at which frequencies possible mode shapes appear. One representative example of a stabilization diagram from the experimental tests is shown below in Figure 7.

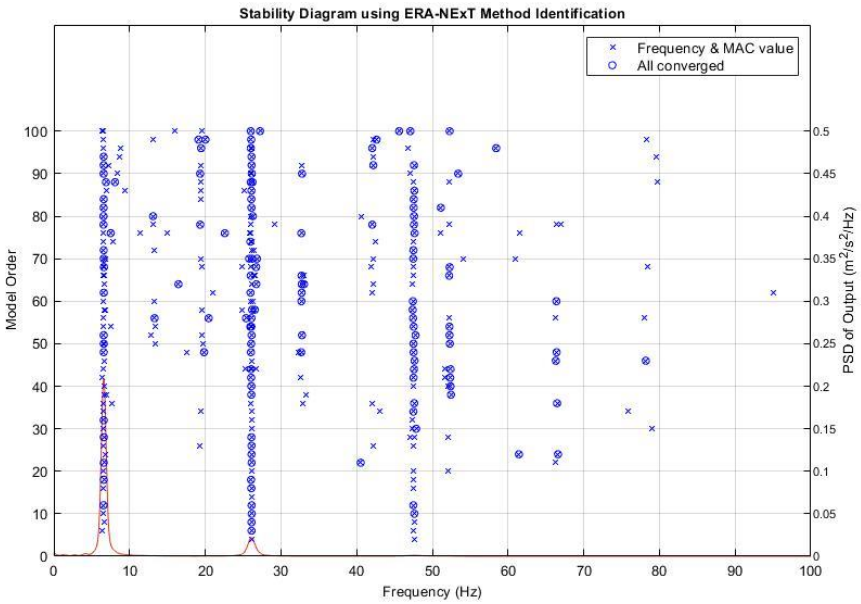

Figure 7: Stabilization diagram

From this diagram, mode shapes can be identified where a vertical column of points is formed at a specific frequency. In Figure 7 above, it is pretty clear that there are three mode shapes, indicated by the three vertical columns in the diagram. The mode shapes and frequencies from this stabilization diagram are shown below in the following figures. Figure 8 shows the first mode shape at a frequency of 6.56 Hz, Figure 9 shows the second mode shape at a frequency of 26.1 Hz, and Figure 10 shows the third mode shape at a frequency of 47.5 Hz.

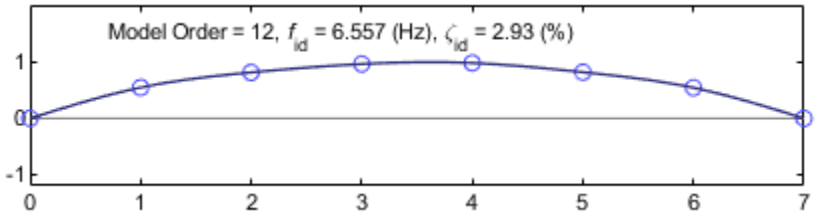

Figure 8: 1st mode shape from stabilization diagram

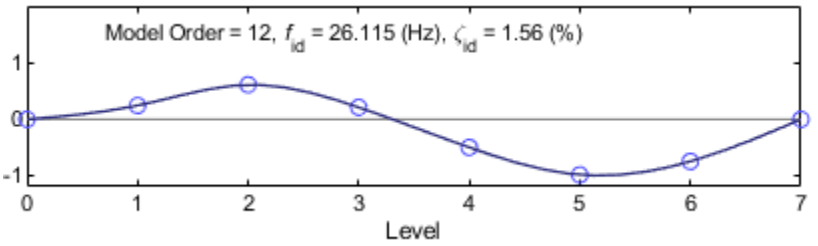

Figure 9: 2nd mode shape from stabilization diagram

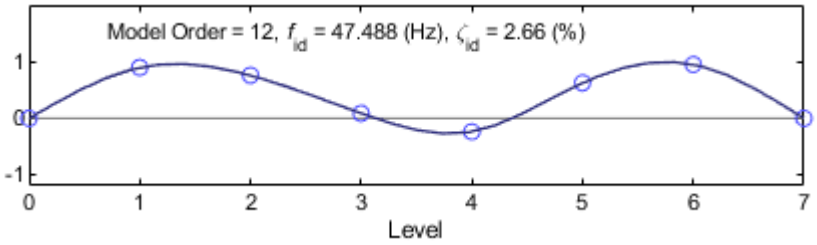

Figure 10: 3rd mode shape from stabilization diagram

Across all of the experimental results from the different loading types, mode shapes 1 and 2 saw consistent frequencies, while mode shapes after 2 could not be confirmed as confidently. Similar frequencies for mode shapes 3 and 4 appeared across many of the test sets, but were not as consistent as the first two modes. Table 1 below summarizes the frequencies for the first four mode shapes as a result of the experimental testing on the TFG specimen.

Table 1: Experimental frequencies for 1st four mode shapes

Mode Shape	1	2	3	4
Frequency (Hz)	6.7	26.3	48	65

As previously mentioned, the frequencies for the modes corresponding to the first ten eigenvalues were extracted from the finite element model to try to match the frequencies in Table 1 above. The FEM frequency results are shown below in Figure 11. As shown in these results, the frequencies for the first and third eigenvalues correspond well with the first two experimental frequencies in Table 1. These matching frequencies suggest that the model of the girder is fairly accurate. However, since the experimental frequencies for the third and fourth mode shapes do not appear to match as well with the FEM results, the model still needs to be adjusted to confirm these results.

X	Frequency (Hz)
1.	7.1155
2.	9.46826
3.	25.2733
4.	43.0171
5.	44.3339
6.	59.1381
7.	71.2772
8.	84.8672
9.	98.5781
10.	101.486

Figure 11: FEM frequency results

5. Future Work

As this study is an ongoing project, there are still many steps to be taken. One of these steps involves adjusting the finite element model to match more of the frequencies obtained through the experimental tests. Matching these results will validate the model and indicate that it is set up correctly and running properly. Another possible step to help validate the model would be to identify other possible mode shapes and corresponding frequencies from the experimental

results. As of now, only the vertical response has been analyzed, so taking into account the horizontal response of the girder may output other modes and frequencies that could be checked against the results of the finite element model. Once the model is validated, dynamic loading will be applied to obtain dynamic response data for the curved girder. This analysis can output both acceleration and strain data, which can be used to train and validate the neural network algorithms. Once the proposed methodology of this project has been confirmed and is working properly on the curved girder, it can be implemented and tested on more complex structures. Additionally, the ultimate goal is to develop a mobile app to record and store acceleration data from the built in accelerometers in smartphones.

6. Acknowledgements

This research was conducted at the Advanced Technology for Large Structural Systems (ATLSS) Research Center at Lehigh University. The Center for Integrated Asset Management for Multi-modal Transportation Infrastructure Systems (CIAMTIS): Region 3 University Transportation Center is acknowledged for sponsoring and providing funding for this project. I would like to thank my research faculty advisors, Dr. Shamim Pakzad and Dr. Martin Takáč, as well as my graduate student mentors on the project team, Sila Gulgec and Soheila Sadeghi Eshkevari.

Works Cited

Chang, Minwoo, and Shamim Pakzad. "Observer Kalman Filter Identification for Output-Only Systems Using Interactive Structural Modal Identification Toolsuite (SMIT)." *Journal of Bridge Engineering*, vol. 19, May 2014, p. 04014002. *ResearchGate*, doi:10.1061/(ASCE)BE.1943-5592.0000530.

Downing, S., and D. Socie. "Simple Rainflow Counting Algorithms." *International Journal of Fatigue*, vol. 4, no. 1, Jan. 1982, pp. 31–40. *DOI.org (Crossref)*, doi:10.1016/0142-1123(82)90018-4.

Gulgec, Nur, et al. *Innovative Sensing by Using Deep Learning Framework*. 2019, pp. 293–300. *ResearchGate*, doi:10.1007/978-3-319-74421-6_39.

Kim, S., et al. "Health Monitoring of Civil Infrastructures Using Wireless Sensor Networks." *2007 6th International Symposium on Information Processing in Sensor Networks*, 2007, pp. 254–63. *IEEE Xplore*, doi:10.1109/IPSN.2007.4379685.

Matarazzo, Thomas, and Shamim Pakzad. *Mobile Sensors in Bridge Health Monitoring*. Vol. 2, 2013.

Putnam, Eric. *Design, Experimental, and Analytical Study of a Horizontally Curved Tubular Flange Girder*. Lehigh University, 2010.

Sen, Debarshi, and Satish Nagarajaiah. *Data-Driven Approach to Structural Health Monitoring Using Statistical Learning Algorithms*. 2018, pp. 295–305. *ResearchGate*, doi:10.1007/978-3-319-68646-2_13.

EFFICIENT SERVICE LIFE EXTENSION OF BRIDGES THROUGH RISK-BASED LIFE-CYCLE MANAGEMENT AND HIGH-PERFORMANCE CONSTRUCTION MATERIALS: EMPHASIS ON CORROSION-RESISTANT STEEL

AUGUST 2, 2019

TRYSTAN GOLDEN
CIAMTUS – UTC - REU

Abstract

Making the most efficient decisions regarding corrosion in our steel structures requires a detailed understanding of the properties of steel materials, the effects of various environmental factors, and the costs and emissions associated with the production of construction materials. By using a life-cycle approach to carbon-dioxide emissions it is possible to model and compare the major sources of carbon-dioxide emissions associated with both A1010 stainless steel and traditional carbon-steel. The importance of repainting schedules is emphasized in previous papers that aimed to compare A1010 stainless steel to carbon-steel but lacked the empirical data to support their assumptions. By using the National Bridge Inventory database to analyze inspection data, it is possible to show the coating life of zinc-primer used on steel bridges is best modeled by a Lognormal distribution with a mean of 15.4 years and a standard deviation of 5.3 years. This information is useful in understanding the total cost and emissions associated with the lifecycle of a carbon-steel bridge, especially when using a probabilistic model. The results of the deterministic model performed in this report show, when comparing A1010 stainless steel to carbon-steel, the initial carbon-dioxide emissions of A1010 steel are 256% larger that carbon-steel at 202.275 tons to 79.05 tons, respectively. When considering indirect sources of emissions from repainting and detouring of traffic during maintenance, however, A1010 stainless steel becomes the cleaner alternative after just a single repainting with total emissions from A1010 steel and carbon-steel being 202.275 ton to 225.20 ton, respectively. This difference will increase further as more than just one repainting is considered.

Background

The corrosion of steel is one of the greatest challenges to our aging infrastructure in the United States. It is reported that corrosion loss accounts for 6.1% of the United States' total GDP, annually (NACE, 1988; G2MT Labs, 2013). Any improvements in the efficiency of using steel materials or with repairing or preventing damage to steel structures has large economic incentives. The exposure of traditional carbon-steel to the air and moisture results in the oxidation of the iron in steel. Overtime, this can result in the reduction of structural efficiency as section loss occurs. The rate of corrosion is a multi-faceted problem that involves the steel material being used, the environmental impacts, as well as the coating type, if any. A thorough understanding of the best ways of repairing and preventing corrosion in large structures is necessary for the safety and efficiency of our infrastructure. Understanding how other steel alternatives compare is important to make the most educated decision on cost and emissions.

A major contender with traditional carbon-steel is A1010 stainless steel and it has already been implemented in numerous bridges across the country. The major difference between the two types of steels is the high chromium content of stainless steel that forms a protective layer on the steel to prevent the fast-acting process of corrosion seen in carbon-steel. While corrosion still occurs in A1010 stainless steel, the onset rate is so slow, there is no need for a paint coating to protect against exposure in a bridge life-cycle (75-125 years). This creates a major difference in how these two types of bridges are maintained after construction. While structural deficiencies still need to be maintained in both types of steel, repainting maintenances, and thus, detouring related emissions and costs do not exist in bridges constructed out of A1010 steel. The major question is whether this absence of emissions and cost makes up for the higher cost of producing and manufacturing A1010 steel compared to carbon-steel? Since the use of stainless steel in

large structures, such as bridges, has just begun, reliable data on the cost and emissions of A1010 stainless steel is sparse and this question cannot be answered without further research.

The two major reports that have compared A1010 steel to carbon-steel are Okasha and Frangopol's "Life-Cycle Cost Analyses of a New Steel for Bridges" in 2012 and Soliman and Frangopol's "Life-Cycle Cost Evaluation of Conventional and Corrosion-Resistant Steel for Bridges" in 2015. Both paper's used Monte Carlo Simulation to model the cost of the two steel alternatives in a bridge. Okasha's paper focused on the direct cost of the steel material as well as the direct costs of the repainting maintenances. Soliman's paper went further to introduce the indirect costs associated with economic and environmental losses due to detouring. Both papers, however, fail to take the approach of a life-cycle environmental assessment to directly compare the emissions of the two types of steel. Furthermore, Soliman uses communication with PennDOT to back up assumptions on the repainting interval of carbon-steel, while both lack empirical data to back up their time-interval assumptions. Since repainting maintenances are seen as the most important difference, outside of initial cost, between the two types of steel bridges it was decided that empirical data should be used to support any time-interval assumptions made moving forward. The application of the life-cycle environmental assessment to quantify emissions from both types of steel and the use of empirical data to support any assumptions on the time-interval of repainting maintenances of carbon-steel bridges will be the main means of differentiating this report from previous ones.

Methods

This report has two main objectives; to form an appropriate and meaningful method of modeling the time-interval between paintings of carbon-steel bridges and to identify and quantify all major carbon-dioxide emission sources in the life-cycles of both A1010 steel and carbon-steel and compare them to one another. Moving forward, each section of the report will be divided into two parts, one for each objective, in order to add clarity to the approach and results. The time-interval shall be discussed first in all sections as it was the objective that was researched first, and the results of time-interval research will contribute to calculating the life-cycle emissions in the second objective.

1. Time Intervals

The Federal Highway Administration supplies annual bridge inspection data through the National Bridge Inventory Database. The data collected through the National Bridge Inventory will be the sole means of analyzing the time-interval between repainting of carbon-steel bridges. Each bridge is rated on a conditional rating scale of 0-9 for each of its three structural components: decking, superstructure, and substructure. A description of each of the ratings is shown in Figure 1 of Appendix A, with 9 being the highest rating and 0 being the lowest, in terms of positive bridge condition. As the coating on the steel-girders degrades and the bridge begins to show signs of corrosion, the conditional rating is expected to decrease. Similarly, when the steel-girders receive a repainting or a replacement, the expectation is that the conditional rating will increase. While the NBI database provides data for all bridges in the United States, using all of that bridge data would be difficult and inappropriate without classifying each bridge according to atmospheric, marine, and de-icing salt exposure. To simplify the approach, only

steel-girder superstructure bridges in Pennsylvania were considered since Pennsylvania is landlocked, meaning there are little to no bridges that will experience marine conditions and all bridges can be grouped into the same level of exposure. Resultingly, any use of the data collected through this method should be applied only to bridges in similar levels of exposure and of the same steel-girder design.

The greatest challenge in using the NBI data is to create an appropriate definition that is consistent with what we want out of the data. There are two major approaches used when considering whether to paint a bridge, reactive and proactive. In the reactive case, any maintenance is the result of direct observation of deterioration in the structure. This case is best represented when we see an increase in the conditional rating of the superstructure. Data collected with this assumption will provide us with the real time interval between when a bridge receives another repainting. On the other hand, the proactive case involves repainting according to a set timeframe that attempts to prevent the exposure of the bridge, and thus corrosion. This case is best represented as the time the superstructure conditional rating stays within a certain range of values. Data collected with this assumption will provide us with an estimate of the coating life of the zinc-primer.

In the reactive case we want to avoid maintenance actions that involve avoid any minor repainting like annual spot-repainting as well as any inconsistencies in inspector's judgement. As a result, an increase in the conditional rating of only 1 is not strong enough to provide confidence that a major maintenance occurred. The definition that was used in this case was when the superstructure conditional rating increases by 2 or more from one year to the next. Any dates of construction or reconstruction were also taken as points of fresh coating. This type of definition is generally safe against inconsistencies in inspector's judgement from year to year as well as

from the types of maintenances that would not result in major detouring of the roadway, which is what we want to identify. Using the descriptions of each conditional rating, as shown in Figure 1, the best range of ratings to represent coating-life would be between 9 and 5. This means that when the superstructure starts at an “excellent” or “very good” condition and begins to show “minor corrosion” as mentioned in the description of conditional rating 5, the coating is considered to be failing, and in need a replacing. This proactive definition is great at representing the true coating life of the zinc-primer used in most bridges and does not have the problem of being subject to monetary constraints like the reactive definition does. It is possible to apply these definitions to all 2545 steel superstructure bridges that had consistent bridge data between 1992 and 2018 on the NBI database. Afterwards, a KS Test will be conducted to see if the data is best represented by the normal or lognormal distribution, or neither. The results will be shown and discussed in the next section.

2. Life-Cycle Environmental Assessment

The E-17-AH bridge in Colorado was the focus of the life-cycle environmental assessment as it provided well-known parameters since it was the bridge used in the case study of Estes paper on reliability theory in structures entitled “Repair Optimization Of Highway Bridges Using System Reliability Approach. A side-view of the bridge is provided in Figure 2 of Appendix A of the report. There are nine steel girders that make up the superstructure of the E-17-AH bridge being analyzed and these will be the focus of LCEA. The interior and exterior girders have different properties due to differences in loading. The exterior girders are W33x125 while the interior girders are larger W33x132 and the details of each girder are shown in Figure 3 of Appendix A of this report. As with all Life-Cycle Environmental Assessments, the process begins with establishing the system boundary according to the goals of the LCEA. Since the

objective is to compare the two types of steels, points of similar emissions can be ignored if they expect to constitute only a minor source of emission. Only the raw material acquisition and production of the nine steel girders will be considered alongside the raw material acquisition and production of the zinc that composes 85% of the primer, and the increased emissions caused by the detouring during a major repainting maintenance (Kogler, 2012). A complete system boundary is adopted in Figure 4 of Appendix A, from a paper by Gervasio and Silva titled "Comparative Life-Cycle Analysis of Steel-Concrete Composite Bridges" from 2008. While this paper focused on composite bridges, the system boundary is still applicable due to its focus on bridge structures. The major sources discussed above are highlighted in Figure 4. All other sources of emissions associated with the decking, substructure, erection, machinery, transportation, non-corrosion related maintenances, demolition, recycling, and landfilling will be ignored either due to their expected similarities between A1010 steel and carbon-steel or to their minor contribution to the overall total emissions in the life-cycle of the bridge.

Once the system boundary is established, a carbon-dioxide inventory can be created to try and quantify how much carbon dioxide is being emitted from each source considered in the system boundary discussed above. Collecting data from various sources it is possible to come up with emission data for the embedded and production emissions of each steel material. The available literature provided many different values for the emissions of carbon-steel, as it is a well-established construction material, however, A1010 stainless steel has very little emission data with only one value being reported by the ISSF report in 2011. All of the values collected are tabulated and shown in Appendix under Table 1., with values separated by production process and country of production where applicable. As shown in Table 1, there are two main types of steel production;/ Basic Oxygen Furnace (BOF) in which new steel is created through

the conversion of pig iron by blowing oxygen through it, and Electric Arc Furnace (EAF) in which steel, usually recycled scrap, is melted down to a liquid and then reformed. Since the two processes have different rates of emissions the proportion of steel made from each process is needed to create a weighted average of the total embedded and production emissions of a steel member. Through communication with Arcelormittal, we learn this proportion is about 33% Basic Oxygen Furnace and 66% Electric Arc Furnace. This information, alongside the weights of each of the two types of steel girders are shown in Table 2 of Appendix A. This report will choose to focus on the bolded values in Table 2., as they are all based upon the production process of steel. Since the only value obtained for stainless steel is based upon a purely Basic Oxygen Furnace Process, we will assume the proportion of stainless steel made through BOF is 100%. All emission values that have a range will use the mean value since the calculations are done through a deterministic approach. Using this information, the embedded and production emissions from the nine steel girders of the E-17-AH bridge can be estimated through a deterministic approach for each steel material and compared.

The emissions associated with embedded and production of the zinc that composes about 85% of the zinc primer used on most bridges is one indirect source that must be accounted for in order to properly compare the emissions of both A1010 steel and carbon-steel (Kogler, 2012). According to the Federal Highway Administration steel design guidebook, the density of the zinc-primer and approximate coat thickness can be estimated. These values are recorded in Table 3 of Appendix A alongside the surface area of the two types of steel girders found in the E-17-AH bridge. Like the embedded and production emissions of the steel girders, the repainting emissions due to the zinc can be calculated deterministically.

The final source of emission that will be focused on in this report are the detour emissions caused by the traffic disruption during a major repainting maintenance. By adopting the equation used by Soliman, we can estimate the indirect environmental impact, in terms of carbon-dioxide, associated with carbon-steel's detouring. All results will be for a single repainting, and by using the time-interval data collected from objective one, it is possible to quantify the total carbon-dioxide emissions of carbon-steel from direct and indirect sources. The equation, along with the necessary variables are shown in Figure 5 and Table 4 respectively.

All the information will be used to carry out calculation that are shown in Appendix B of this report. The next section of the report will discuss the results of these calculations and see which option, if either, is the cleaner option.

Results and Discussion

1. Time Intervals

After applying definition 1 (reactive assumption) to all 2545 steel superstructure bridges in Pennsylvania that had inspection data from 1992 to 2018, 75 bridges provided time intervals between what were considered repainting actions. The histogram of the time-interval between repaintings for definition 1 is shown in Figure 6 of Appendix A, while the data plotted against the normal and lognormal distributions is shown in Figure 7. The data had a mean of 15.8 years and a standard deviation of 6.99 years. A KS Test shows the data is best represented as a normal distribution with a p-value of .374 while the p-value for the lognormal distribution was .0434.

When definition 2 (proactive assumption) was applied to all 2545 steel superstructure bridges in Pennsylvania that had inspection data from 1992 to 2018, 128 bridges provided time-intervals that represent the coating life of the zinc-primer. The histogram of the coating life span for definition 2 is shown in Figure 8 of Appendix A, while the data plotted against the normal

and lognormal distributions is shown in Figure 9. The mean coating life span was 15.4 years and the standard deviation was 5.3 years. The KS Test shows the coating life is best modelled by a lognormal distribution with a p-value of .1113 while the p-value for the normal distribution is .0946.

There are major concerns whether definition 1 (reactive assumption) can provide reliable data on the time-interval between repaintings. Table 5 provides a list of value found through literature review of estimates of repainting intervals as well as coating life estimates. Since the data collected is representative of Pennsylvania the intervals cited by Soliman through PennDOT communications should give the best indication of whether definition 1's data is reliable or not. Since PennDOT reports repainting intervals are between 30 and 50 years for initial coatings and 20 to 30 years for subsequent coatings, it creates serious doubt as to whether the mean of 15.8 years for definition 1 is accurate or not. Furthermore, if the real mean interval is in the upper twenties, there isn't enough inspection data between 1992 and 2018 (26 years) to capture the real time intervals between repainting of bridges with exposure levels similar to Pennsylvania bridges. Lastly, any value obtained using definition 1 would be a low-bound estimate since over three-fourths of bridges that were analyzed with definition showed no signs of even a single repainting maintenance, let alone the two required to create a time-interval.

The values obtained for definition 2 (proactive assumption) seem to match the value obtained from The Federal Highway Administration (FHWA) of 15-25 years. If the coating life is to be used in future modelling it should be noted that real repainting maintenances occur according to definition 1 and not definition 2, meaning unless it is known that a bridge owner follows a proactive maintenance schedule, using definition 2 will overestimate the number of repaintings a bridge will receive in its life-cycle.

2. Life-Cycle Environmental Assessment

The results of the life-cycle environmental assessment provide interesting results that serve as a preliminary analysis into the relative emissions of both A1010 stainless steel and carbon-steel. Since the true emissions values are unknown and there isn't enough evidence to justify using the mean value of the ranges in Table 1, the results of the deterministic analysis should serve only as an indication of the true carbon-dioxide emissions from the life-cycle of nine steel girders used in the E-17-AH bridge in Colorado.

That being said, the calculations shown in Appendix B and their respective results shown in Tables 6, show promising results for A1010 stainless steel. As is easier to see in Figure 10, the initial carbon-dioxide emissions of A1010 stainless steel are much higher than carbon-steel at 202.275 tons to 79.05 tons, respectively. Once the repainting and detouring emissions are considered, however, the total carbon-dioxide emissions from carbon-steel becomes greater than that of A1010 stainless steel after just one repainting. The values of the emissions for both steels after a single repainting is shown in Figure 11. As can be seen, within a few decades (15-30 years), after the carbon-steel bridge is repainted for the first time, A1010 steel becomes the cleaner option in terms of carbon-dioxide emissions. This difference will only grow as the number of repaintings considered is increased. In a typical life-cycle of a steel girder bridge (75-125 years), it is not uncommon to see three to five repaintings, especially considering the results from objective one of this report.

Summary and Conclusions

There is still a need to perform further research in the area of A1010 stainless steel to fully understand the full cost and emissions associated with this new structural material. The results from objective 1, did not provide the conclusive results the team had hoped for in order to represent the real

time-interval between repaintings of Pennsylvania bridges. Using NBI data to represent the real time-interval between repaintings was not an appropriate method since there were only 26 years of data and the suspected time-interval between repaintings is expected to be between 20 and 30 years. Due to the lack of inspection data going back over 30 years, a different approach should be used to collect data on repainting intervals in the future. However, the results obtained to represent the coating life of zinc-primer used to protect carbon-steel from corrosion seem to be reliable when compared to the estimated coating life provided by the Federal Highway Administration. Of 2545 bridges analyzed 128 bridges provided coating life spans with a mean value of 15.4 years and standard deviation of 5.3 years. This data is shown by a KS Test to best be modeled as a lognormal distribution with a corresponding p-value of .1113. The second objective of the report, to perform life-cycle environmental assessment using a deterministic approach, suggests the carbon-dioxide emissions of A1010 stainless steel throughout its life-cycle is lower than that of carbon-steel, especially when considering multiple repaintings. The total carbon-dioxide emissions of carbon-steel after a single repainting are 225.20 tons while A1010 steels emissions are lower at 202.275 tons.

It is my hope that this report will provide motivation for more research to be conducted in the future on the feasibility of using A1010 stainless steel in structures such as bridges. It is suggested that a probabilistic approach should be used, and all variables used in this report given statistical models with proper justification. This report made oversimplifications in order to use a deterministic approach and provide quicker results which can be corrected using a probabilistic model. Hopefully, the results of the coating life of zinc-primer from definition 2 (proactive assumption) from objective 1 can be used as a more reliable source in probabilistic models compared to what has been used in previous papers.

Acknowledgments

I would like to thank all members of my research team; Dr. Frangopol for allowing me to conduct research in his area of expertise as well for helping me better prepare for my future career in Civil Engineering. David Yang for giving me strong guidance throughout the research process. It would have been impossible for me to accomplish as much as I did without his help. Cheng Yuan for providing much of the framework for the research I performed. Much of the approach in this report came from his ideas and I am happy I had the opportunity to adopt his model and perform the preliminary work in the area. Xu Han for working alongside me throughout the summer and for providing me with challenging questions and critiques to my approach along the way.

I would like to thank all the faculty and staff of ATLSS that made the REU program possible including but not limited to; Chad Kusko for directing the program and offering guidance throughout the summer as well as being someone to talk to about my future in Civil Engineering. Peter Bryan for offering technical support whenever needed as well as being someone to make me laugh.

I would like to thank all other members of the REU and NHERI program that made the summer unforgettable.

Works Cited

Dusart, Antoine, et al. *ISSF Report*. ISSF, 2011. Print.

Fletcher, Fred. *Improved Corrosion-Resistant Steel for Highway Bridge Construction*. FHWA-HRT-11-062 Vol. Georgetown PA: Federal Highway Administration, 2011. Print.

Genderen Van, Eric, et al. "A Global Life Cycle Assessment for Primary Zinc Production." *The International Journal of Life Cycle Assessment* 21.11 (2016): 1580. Print.

Kogler, Robert. *Steel Bridge Design Handbook: Corrosion Protection of Steel Bridges*. FHWA-IF-12-052 - Vol. 19 Vol. , 2012. Print.

Okasha, Nader; Frangopol, Dan. 2012. Life-Cycle Cost Analyses of a New Steel for Bridges.

Soliman, Mohamed; Frangopol, Dan. 2015. Life-Cycle Cost Evaluation of Conventional and Corrosion-Resistant Steel for Bridges.

Appendix A: Tables and Figures

9	EXCELLENT CONDITION
8	VERY GOOD CONDITION - no problems noted
7	GOOD CONDITION - some minor problems.
6	SATISFACTORY CONDITION - structural elements show minor deterioration
5	FAIR CONDITION - all primary structural elements are sound but may have minor corrosion, cracking or chipping. May include minor erosion on bridge piers.
4	POOR CONDITION - advanced corrosion, deterioration, cracking or chipping. Also significant erosion of concrete bridge piers.
3	SERIOUS CONDITION - corrosion, deterioration, cracking and chipping, or erosion of concrete bridge piers have seriously affected deck, superstructure, or substructure. Local failures are possible.
2	CRITICAL CONDITION - advanced deterioration of deck, superstructure, or substructure. May have cracks in steel or concrete, or erosion may have removed substructure support. It may be necessary to close the bridge until corrective action is taken.
1	"IMMINENT" FAILURE CONDITION - major deterioration or corrosion in deck, superstructure, or substructure, or obvious vertical or horizontal movement affecting structure stability. Bridge is closed to traffic but corrective action may put back in light service.
0	FAILED CONDITION - out of service - beyond corrective action
N	Not applicable

Figure 1. National Bridge Inventory Conditional Rating Scale

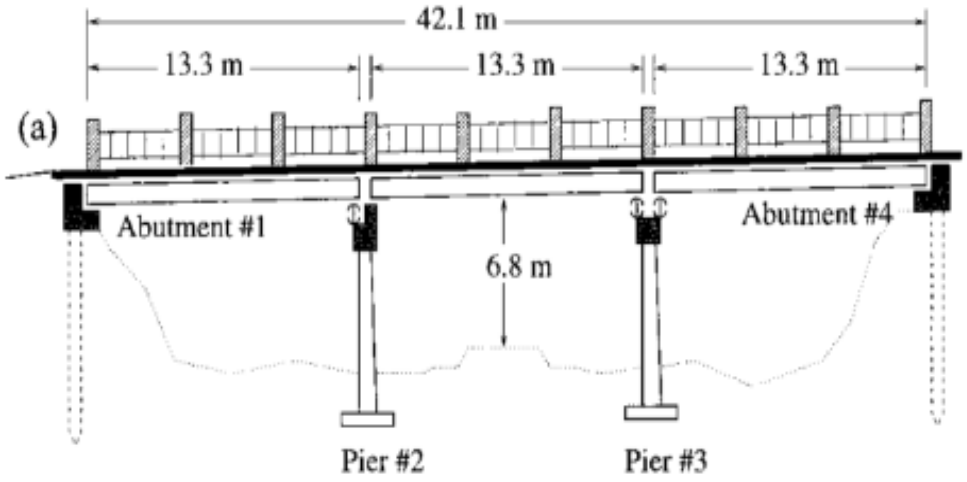

Figure 2. Side View of E-17-AH Bridge in Colorado

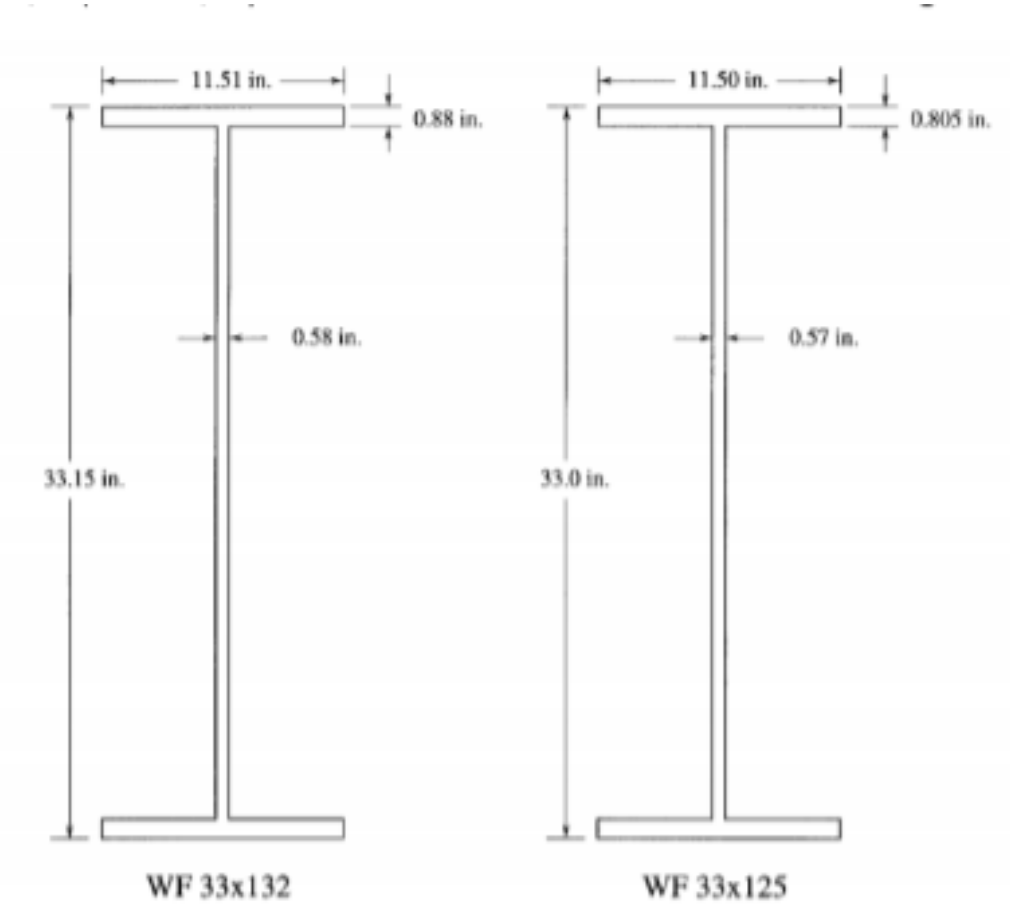

Figure 3. Exterior (right) and Interior (left) Girders of E-17-AH bridge.

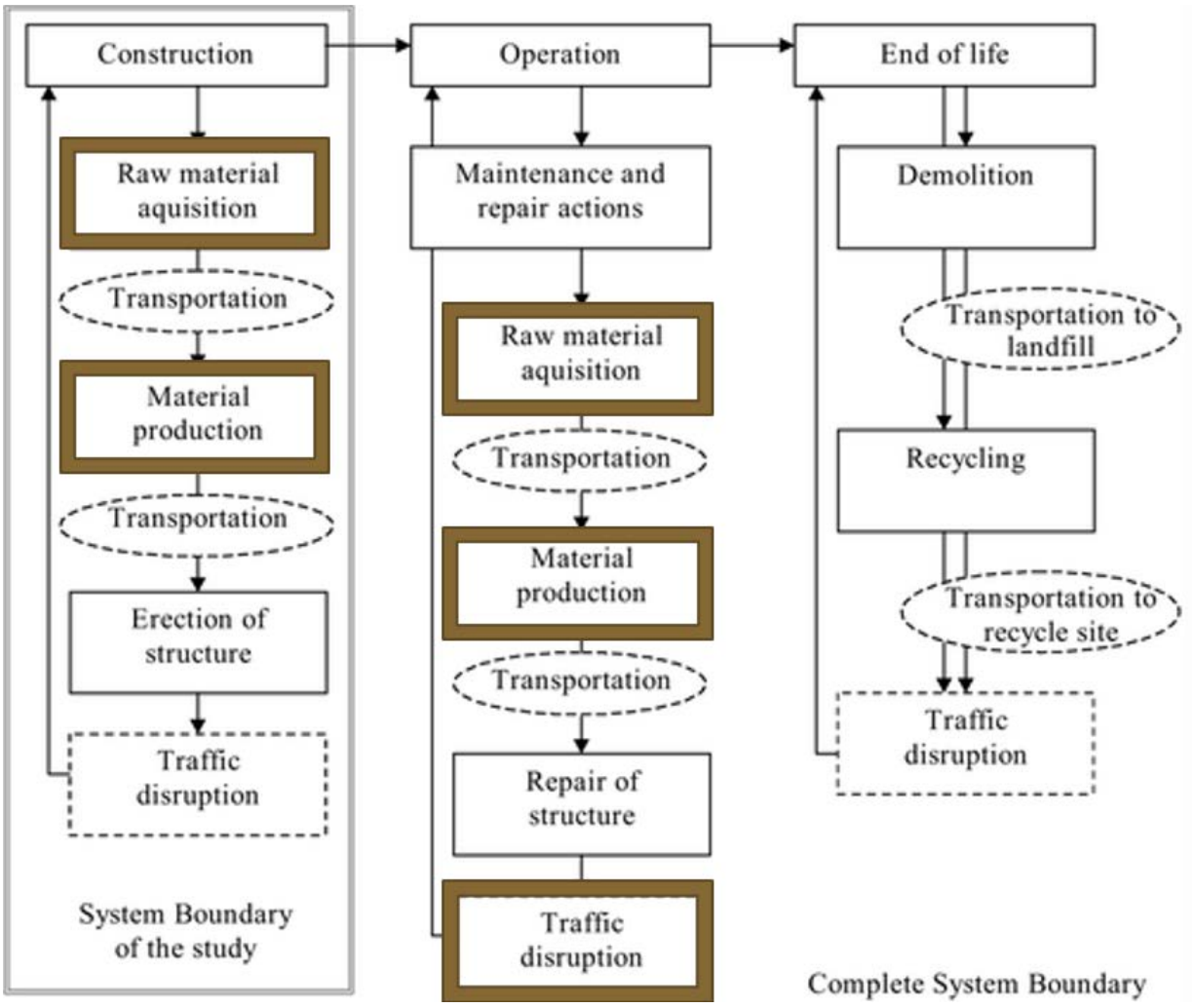

Figure 4. Gervasio's and Silva's Modified Complete System Boundary

Table 1. Carbon-Dioxide Inventory

CO2 Inventory	Value (ton/ton of steel)	Reference
Carbon Steel	1.83 average	World steel association (2017,world)
	1.9 average	Kundak, Mijo, Lad islav Lazić, and Josip Črnko. "CO 2 EMISSIONS IN THE STEEL INDUSTRY." Metalurgija 48.3 (2009).
	1.6-2.2 BOF	International energy agency (IEA) (2011, world)
	1.4-2.0 EAF no scrap	
	0.6-0.9 EAF with scrap	
	2.148 china	Hasanbeigi, Ali, et al. "Comparison of energy-related carbon dioxide emissions intensity of the international iron and steel industry: case studies from China, Germany, Mexico, and the United States." (2015).
	1.708 Germany	
	1.736 USA	
	1.080 Mexico	
Stainless Steel	**2.9 BOF**	ISSF report (2011)

BOF: Basic Oxygen Furnace EAF: Electric Arc Furnace

Table 2. Girder Weights and Steel Production Proportions

Description	Value	Units
Weight Interior Girder		
Weight Exterior Girder		
Total Weight of 9 Girders	69.75	Ton
Proportion Steel Made Through BOF	33	%
Proportion Steel Made Through EAF	66	%

Table 3. Girder Surface Areas and Repainting Propertiesc

Description	Value	Units
Surface Area Interior Girder	1250.78	Ft^2
Surface Area Exterior Girder		
Total Surface Area of 9 Girders		
Coat Thickness		
Primer Density	3.032	Kg/L
CO2 Emissions/ ton Zinc	2600	Kg

$$E = \mathrm{ADT} \cdot l \cdot d \cdot \left[En_{d,c} \cdot (1 - T) + En_{d,t} \cdot T\right] \frac{En_{S_D} - En_{S_o}}{En_{S_o}} \quad (3)$$

Figure 5. Soliman's Equation to Determine Increased Emissions From Detouring

Description	Variable	Value	Units
Average Daily Traffic	ADT	53000	Vehicles/Day
Length of Detour	*l*	1.609	Km
Duration of Maintenance	D	15	Days
Proportion of Trucks to Total Traffic	T	.12	NA
Environmental Metric per unit distance for cars	$En_{d,c}$	.22	Kg Co2/km
Environmental Metric per unit distance for trucks	$En_{d,t}$	.56	Kg Co2/km
Environmental Metric per kilometer at restricted speed S_D	En_{SD}	.416	Kg Co2/km
Environmental Metric per kilometer at unrestricted speed S_O	En_{So}	.298	Kg Co2/km

Table 4. Variables for Detour Emissions based upon Soliman's paper

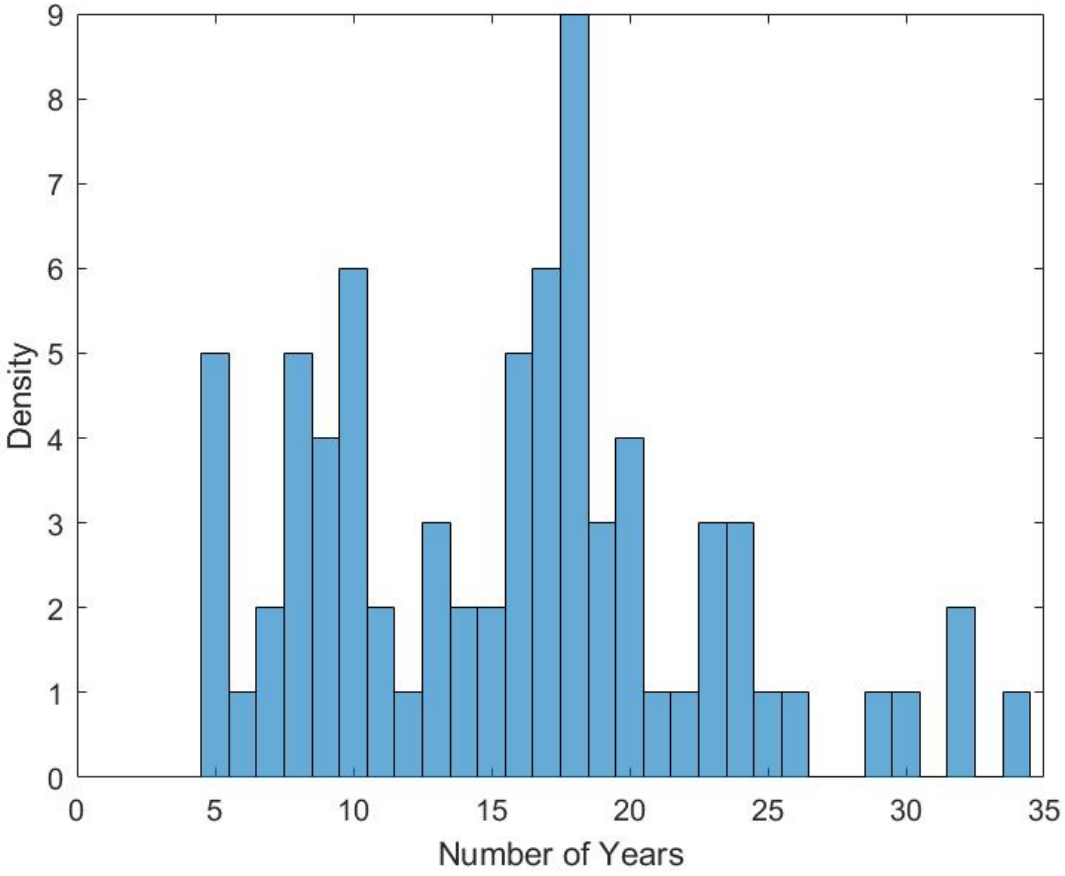

Figure 6. Histogram of Time Intervals for Definition 1 (Reactive Assumption)

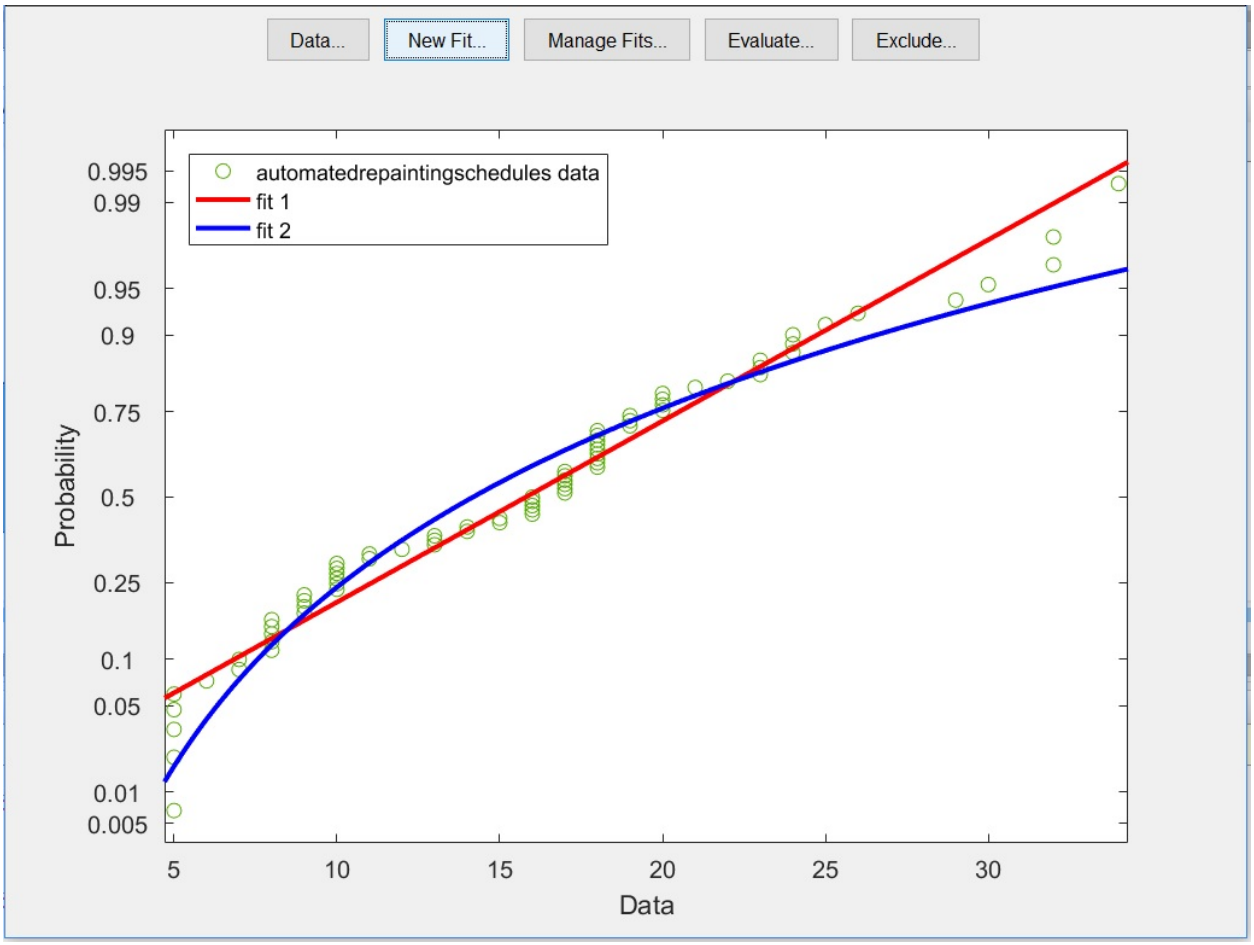

Figure 7. Definition 1 Time Intervals Plotted Against Normal and Lognormal Distributions

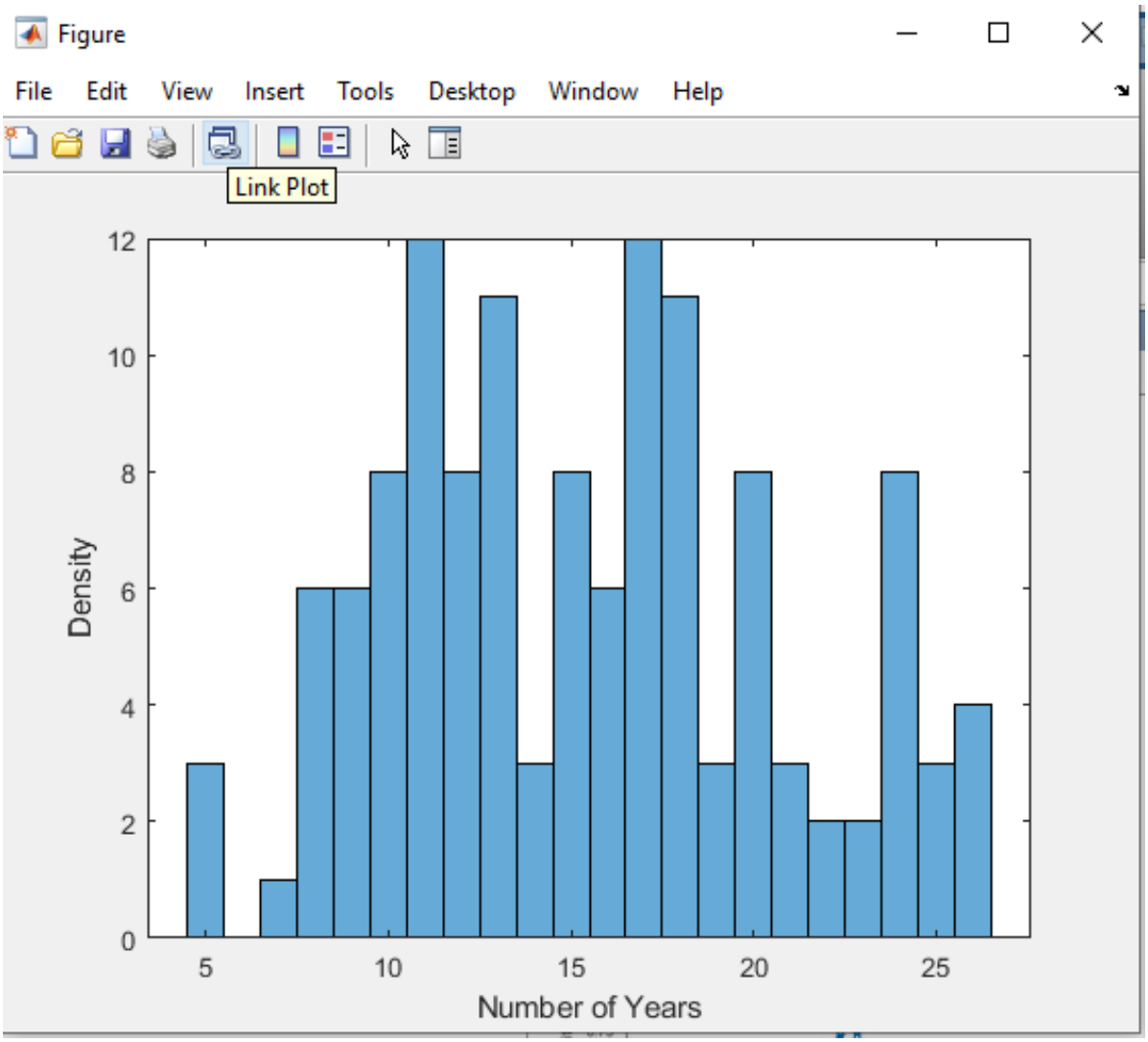

Figure 8. Histogram of Coating Life Span for Definition 2 (Proctive Assumption)

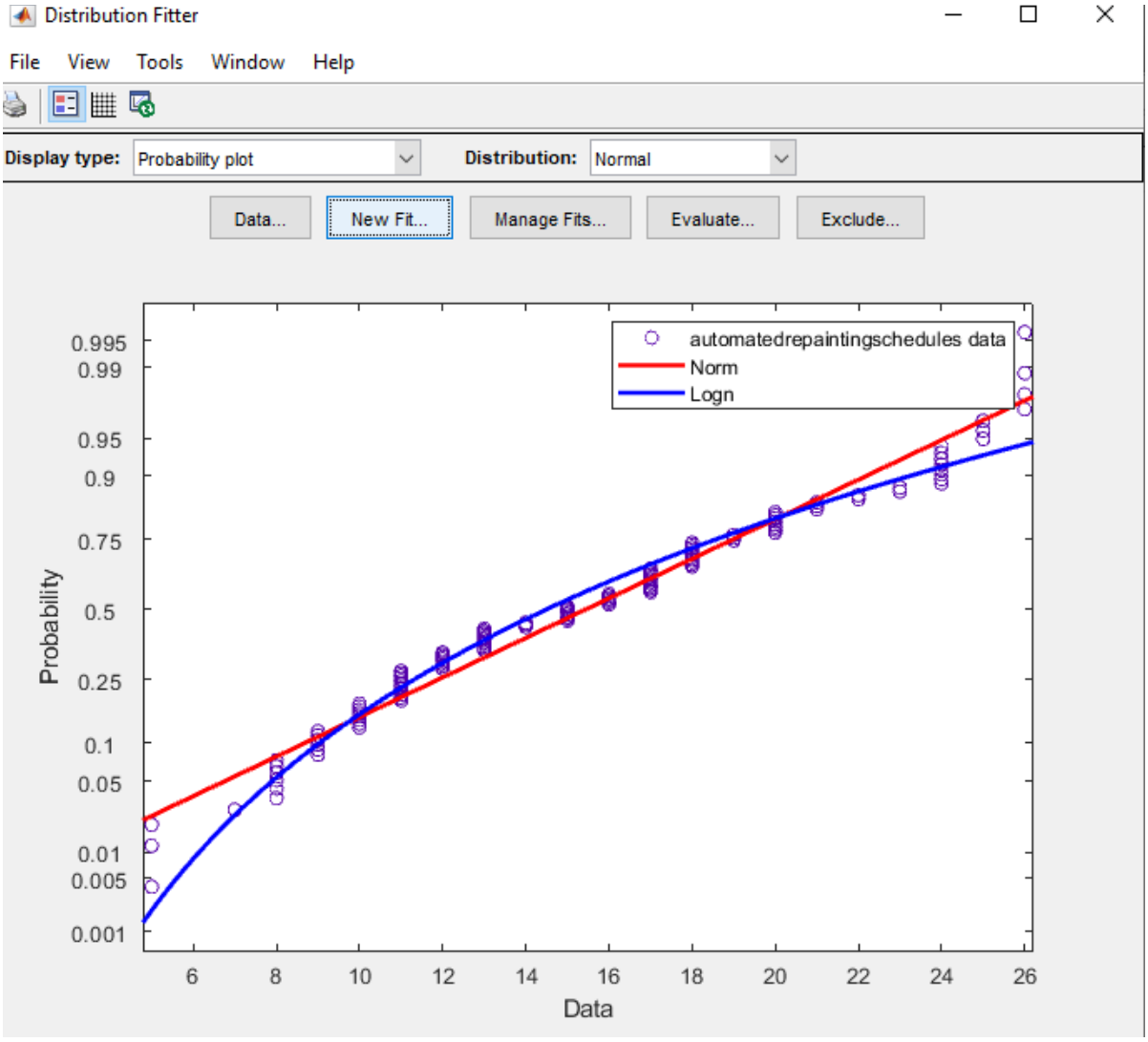

Figure 9. Definition 2 Coating Life Spans Plotted Against Normal and Lognormal Distributions

Table 5. Previous Estimation of Time Intervals Between Repaintings and Coating Life

Source	**Distribution**	**Mean/ C.O.V.**	**Environment**
Maunsell Ltd, Transport Research Laboratory. Optimum maintenance strategies for different bridge type: Bridge data. Final report. London: The Highways Agency; 2000	Normal	20 / .25	None Specified
Source	**Distribution**	**Limits**	**Environment**
Okasha, Frangopol	Triangular	(10,15,20)	Coastal Regions
Source	**Distribution**	**Limits**	**Environment**
Soliman, Frangopol. –PENNDOT, personal communication.	1. Triangular 2. Triangular	(30,40,50) First (20,25,30) Subseq.	Pennsylvania Roads
Source	**Paint Type**	**Mean**	**Environments**
FHWA	Zinc-Rich Primer	1. 15-20 2. 25	1.Marine 2. Salt-Containing
FHWA	Zinc and Zinc/Aluminum Alloy	1. 20-25 2. 40+	1. Marine 2. Salt-Containing

Table 6. Emissions Values From Each Source in Life-Cycle

Description	Value	Units
9 Carbon Steel Girders		
9 Stainless Steel Girders		
Repainting Emissions (PER REPAINTING)	.5382	Ton
Detour Related Emissions (PER REPAINTING)	145.61	Ton

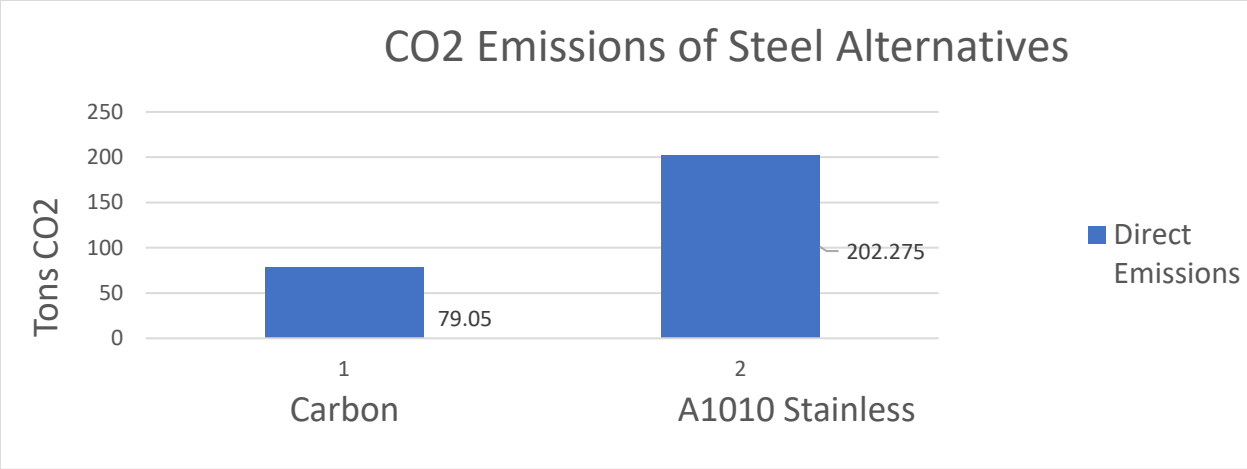

Figure 10. Embedded and Production Emissions of Steel

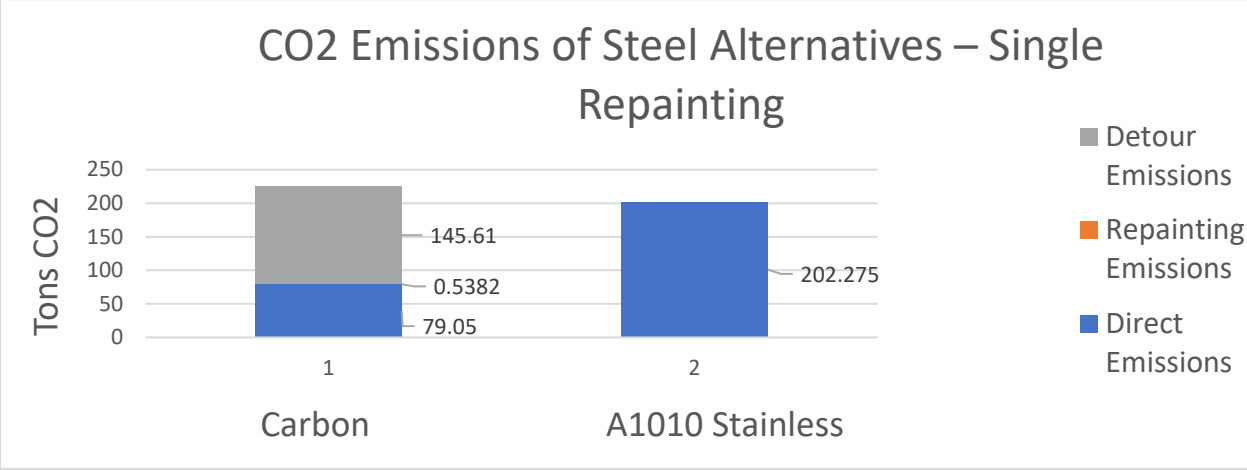

Figure 11. Total Emissions For Both A1010 Stainless and Carbon Steel

Appendix B: Calculations

Embedded and Production Emissions of 9 Steel Girders

- 9 Carbon Steel Girders

  $[(33\%)\left(1.9\frac{Ton\ CO2}{Ton\ Steel}\right)+(66\%)(.75\frac{Ton\ CO2}{Ton\ Steel})](69.75\ Ton\ Steel)$ = **79.05 ton CO2**

- 9 Stainless Steel Girders

  $\left(2.9\frac{Ton\ CO2}{Ton\ Steel}\right)(69.75\ Ton\ Steel)$ = **202.275 ton CO2**

Repainting Emissions

- Primer Needed:

  (11231.81 Ft^2)(.00025 Ft) = 2.808 Cubic Ft. (80.148 L)

- Weight of Primer Needed

  (80.148L)(3.032 Kg/L) = 240.01Kg

- Weight of Zinc Needed

  (.85)(240.01 Kg) = 206.56 Kg (.207 Ton Zinc)

- Emissions

  (2600 Kg/Ton Zinc)(.207 Ton Zinc)**= 538.2 Kg (.5382 Ton) CO2 PER REPAINTING**

Detouring Emissions

- $(53000\ \frac{vehicles}{day})(1.609\ km)$(15 days)$[(.22\frac{Kg\ CO2}{km})$(1-.12) +$(.56\frac{Kg\ CO2}{km})$(.12)$]$ $(\frac{(.416\frac{Kg\ CO2}{km}-.298\frac{Kg\ CO2}{km})}{.298\frac{Kg\ CO2}{km}})$ = **145.61 Ton CO2 PER REPAINTING**

Road Pavement Condition Monitoring by Embedded Crowdsensing

Center for Integrated Asset Management for Multi-modal Transportation Infrastructure Systems (CIAMTIS): Region 3 University Transportation Center

Charles Inwald

Background

The task of detecting, classifying and tabulating data of pavement conditions is a very tedious task. With 4.18 million miles of road in the United States[1], it is intuitively time consuming and cost intensive to effectively monitor the conditions of such a large transportation network. Seventy seven percent of this mileage is maintained by local governments, nineteen percent to state, four percent to federal.[1] Nationwide, over nineteen percent are in poor condition and require repair, which consequently leads to expenditures of $160 billion a year in congestion and delays.[1] From this, is an extra 3.1 billion gallons of fuel wasted.

Given this, it is essential that we act now than later, with every $1 we spend now eliminates or delays spending $10 on rehabilitation or reconstruction later.[2] We currently employ many modern marvels to accomplish these savings on the rough 80 percent of roads that are currently in satisfactory condition, of course discounting the third of all roads that are unpaved gravel or dirt.[1,2] Of the remaining roadways under consideration, fractions are randomly selected for monitoring, leaving the remainder unmonitored. Thus advancements in the efficiency of the methodology of our monitoring has the potential to either extend coverage while maintaining current expenditure, or maintain constant coverage while reducing expenditure.

Abstract

With consideration to the aforementioned near astronomical figure of $160 billion in tangible consequences of congestion and delays, as well as the 90% savings margin that preemptive measures bring, we derive significant interest in “crowdsensing” pavement monitoring. “We”, referring to stakeholders in the transportation network, as any user of the nation’s roadways to any extent has a vested interest in its livelihood, in addition to the government and commercial entities that actively invest in its maintenance. Mobile crowdsensing is the umbrella term for the idea of individuals, or rather “crowds”, contribute data through “sensing”, for the common interest.[3]

This paper aims to explore the implementation of mobile crowdsensing via a cross platform app for smartphones that enables this flow of data, the systems this app depends on, the concept and feasibility of incentive mechanisms to generate stakeholder engagement, as well as the intersection of blockchain and machine learning technologies. Implications of these concepts, assumptions and considerations of the syntax and semantics of this research will also be discussed.

Preventative Maintenance Philosophy and the Pavement Life Cycle

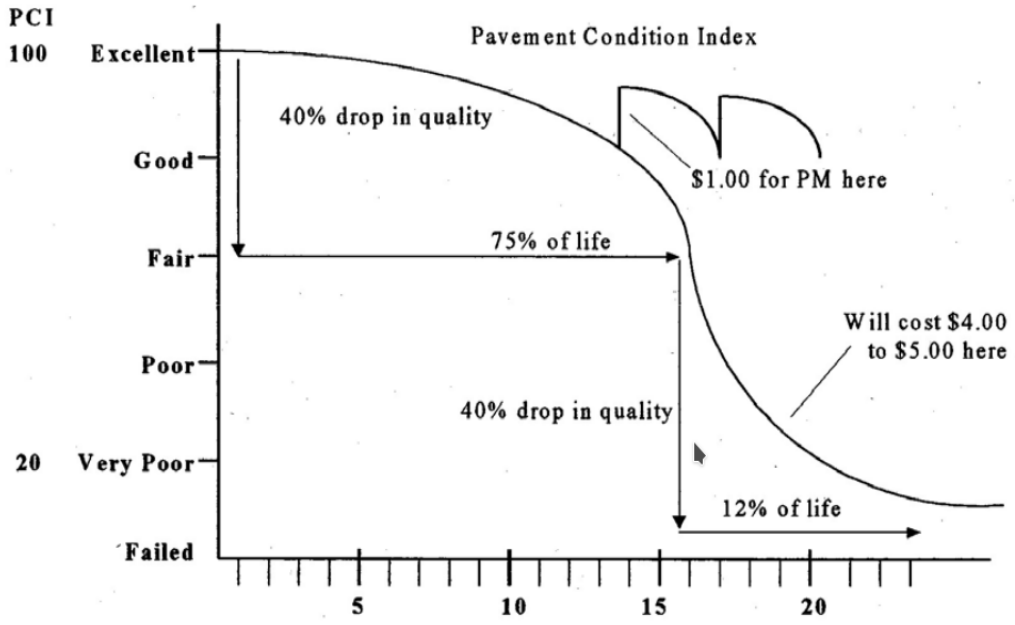

Figure 1: Typical Pavement Lifecycle [4]

As shown in Figure 1, the degradation of pavement does not occur at a linear rate, but rather at a slope that warrants deliberate attention to its behavior in order to optimize effectiveness. Pavement Condition Index, or PCI, is a metric of the condition of a road surface, rated from one to a hundred.[5] The condition factors in the type and magnitude of distresses, including cracks and potholes, as well as the overall roughness of the road.[5] One can deduce from Figure 1 that preventative maintenance is more effective than corrective maintenance when timed correctly, as cost of maintenance quadruples during the latter stages of the lifecycle once the PCI becomes poor.

Current Preventative Maintenance Methodology

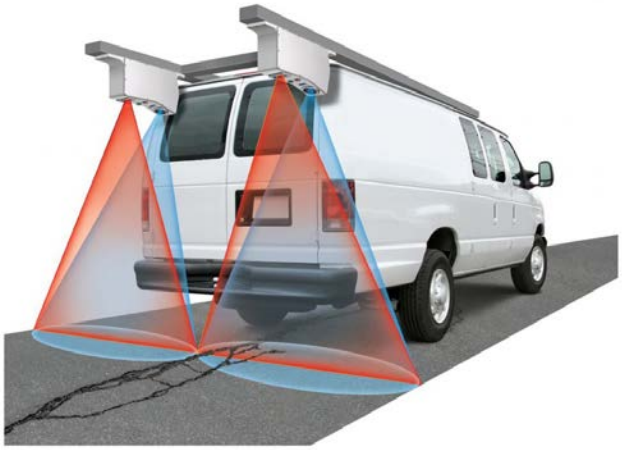

Figure 2: A Laser Crack Measurement System equipped van[10]

Laser Crack Measurement Systems (LCMS) are currently employed in many pavement management systems.[6] This technique makes use of a variety of lasers, optics and cameras to procure troves of data, such that 3D models of the pavement surface are generated.[6] These LCMS are mounted on vans, shown in Figure 2, that can generate 200 kilometers of coverage per day, and can operate in both night and daytime conditions. While LCMS technology is effective, it is constrained by cost and time, and as a result, is relatively rare. The avoidance of these bottlenecks is the motivation behind the implementation of a crowdsensing pavement monitoring system. Such an implementation is spared several expenditures. The crowdsensing approach does not require the initial investment of procuring vans, the state of the art laser and optics hardware to mount on the vans, the time and salary of drivers driving with the sole purpose of monitoring pavement, and the fuel expenses of operating the vans.

Cross Platform Mobile App Development

In order to maximize the population of participants in the crowdsensing network, the mobile client app was designed to be cross platform, that is the app can be run on Android or iOS smartphones. The app is capable of capturing images of road conditions and uploading corresponding sensor data, which is then utilized by a machine learning image classification algorithm, and an administrative dashboard.

Much of the difficulty experienced early on resulted from the nature and architecture of the React and React Native frameworks. React is a web development framework, and React Native is a cross platform mobile app development framework built upon React.[7] The web and mobile app development industries are notorious for "framework churning", which is the constant cycling of libraries, tools, design patterns and philosophies every few months to years. As a result, academic institutions tend to avoid teaching these frameworks as the lessons will lose their value in a few years time.

Consequently, this generally leaves the websites Github and StackOverflow to turn to should issues arise. The unavailability of support on a particular library in React Native, which used a model that prioritized support based on a donation platform, proved to be extremely detrimental to the progress and workflow of the project. The package had no alternatives within the domain of React Native, and was rather fundamental to the project, so the mobile app was rebuilt several times over, finally using Flutter as a workaround to React Native. Over the course of a few short days, rapid progress was made, soon outpacing the original prototype. While many of the abstractions in these frameworks for cross platform development seem to cause more issues than they are worth, at the end of the day the value they bring is determined by

the relative burden of having a code base in multiple programming languages. As this is only the beginning of the code base, keeping scalability in mind is imperative. While React Native itself, along with many of its peripheral libraries like Redux, certainly promote scalability given their deliberate attention given to state management and lifecycle, they prove to be overkill for the purposes of this project. This paired with a troublesome package, led to the disparity in efficiency in working with the respective programming languages.

Backend Development

Backend development is the generation of the server side code and infrastructure that powers the mobile client app and administrative dashboard from behind the scenes. This includes processing the flow of data received from smartphones, storing this data in a structured manner that can be easily queried or manipulated, as well as the hosting and business logic of the administrative interface. The backend is written in Javascript, using the Node.js runtime. Javascript is a programming language, traditionally meant for use in web browsers.[8] The Node.js runtime is what allows Javascript to be run in a context other than the web browser. Using a package called Express, Node.js can act as a full fledged web server, to rival those written in languages like Java, PHP or Python. Express is considered "middleware", managing the input and output of communications between the data processing element of the backend, and the data that is sent to and received from users.

When the backend receives the crowdsensed images and sensor data, it stores it for use by the machine learning image classification algorithm and administrative

dashboard. The machine learning algorithm, written in Python, is called upon and ran by the Express middleware. The backend also has a feature of processing GPS coordinate data into sets of streets, representing the abstraction of a trip that the user took from origin to destination. This is a potential avenue for analysis of how road closures and other changes in the transportation network will affect its users.

Blockchain Integration Proposal

Blockchain, in short, as its name implies, is simply a linked list (chain) of blocks. The blocks are groups of records, which are linked together using cryptography. By design, the idea of blockchain is a distributed ledger that inherently is immutable. It's immutability proves advantageous in the application of Bitcoin, as Bitcoin solves the double spend problem, the first to do so in a distributed manner. The double spend

problem is intuitively when someone manages to spend the same dollar twice, which causes inflation. Traditionally, centralized systems would be responsible for preventing this, and these central authorities would be the single points of failure. Blockchain, while more computationally expensive than traditional databases, comes with the advantage of distributing the burden of preventing the double spend problem, along with other policies, among all the nodes in the network.

Blockchain, in recent times, has arguably been overpromoted to businesses, as a snake oil solution to "revolutionize" just about every industry. A notable example of a firm taking advantage of the hype of blockchain was beverage company Long Island Iced Tea, whose stock jumped 200% when they changed their name to "Long Blockchain Corp" during the bitcoin boom.[9] This was a wakeup call for investors who were simply throwing money around everything surrounding blockchain and cryptocurrency.

It is imperative that we apply blockchain only where it is appropriate. Fundamentally, that determines when we want to decentralize. This makes a lot of sense for currency, since money doesn't need to change or update, hence it is immutable. As aforementioned, the double spend problem is eliminated, which justifies the immense electric bill that cryptocurrencies' require. Prior to migration to a blockchain based system, it should be asked whether the use case benefits significantly from a decentralized approach. In many cases, the costs outweigh the benefits, most notably the electricity used by the network and the investment in development and adoption of the system among other things.

As for the use of blockchain in the crowdsensing of pavement monitoring, the main value add derives from the intersection between machine learning and blockchain. With a centralized model, the central system is responsible for procuring the graphics processing power to run the machine learning algorithm on all the images to be processed. Initially, this system began with a centralized system prior to several realizations. The machine learning image classification algorithm, like most modern ML algorithms, runs best on a discrete GPU, which the in house server did not have. While capable of getting the job done on some number of images needing to be processed, this would not scale well.

A decentralized approach, however, can potentially accomplish two improvements in these regards. A “bring-your-own-GPU-and-algorithm” policy would simply “crowdsource” the two resources that are bottlenecks in the design. A model where participants compete to see who can have the best algorithm and/or GPU, in exchange for cryptocurrency reward. In this scenario, there is no longer any need to amass any significant hashing power in house, and the algorithm no longer needs to be developed in house. ML algorithms “learn” from the data they process, so here both the data and the algorithm are crowdsourced. For example, if a participant’s ML algorithm can correctly classify the entire blockchain of images of road conditions so far as well as some X number of additional images that are to be added to the dataset, and is also the first to do so, the participant is rewarded. This way the ML is constantly improving its own substance and expanding its data set, with its computational labor being fully distributed among its participants.

This system is not, however, free of responsibility. Given the nature of a model that compensates based on contribution, there will of course be users who seek to cheat. For example, a user could potentially use supply fake images from outside the official client app, leading everyone to believe there are potholes where there aren't any. To prevent this, the client app and blockchain system will need to have measures in place to ensure the integrity of the input data. One potential avenue to pursue this with, is by having the client app embed a unique signature using one-way cryptography, so that every node in the network can verify that the origin of the image was the official client app. Adam Hemlin Billström and Fabian Huss, for their master's thesis, were able to construct a blockchain that was able to verify the integrity of videos recorded from an Android device, with a 98.1% accuracy, thereby proving that such a measure is possible.[11]

A chain is as strong as its weakest link, and the blockchain is no exception. If someone were to compromise the integrity of the system, they could very well automate its exploitation, and rapidly amass ill gotten cryptocurrency, which is why the sanitization of the initial input of images is crucial.

Decentralized & Collaborative AI on Blockchain Proof of Concept

Ethereum, one of the larger cryptocurrencies, is known for its distributed application (dApps) platform.[12] The underlying blockchain for this project has so far been implemented using a private Ethereum network. Participants can mine, and thereby process research data, by running an Ethereum compatible “full node”. Nodes are “full”, if they enforce all rules of the network. Participants can act as a full node for this project by using any Ethereum full node software, however this project has been tested using Geth, which is a command line interface written in Go.[12] The project’s private Ethereum network supports transactions, so participants can freely move the project’s generic currency in the same manner as one would send official Ethereum

cryptocurrency, using either Ethereum compatible wallet software, or from the command line.

From full node software, participants can process whatever machine learning workload is propagated to it. To test this capability and assess its feasibility for the proposed goals of this project, the network was test driven using a publicly available IMDB sentiment classifier distributed by Microsoft[13]. Using the React dashboard, a workload can be added to the blockchain, and participants who are mining can supply a sentiment prediction in exchange for reward. Given that the underlying blockchain is not bound to any particular machine learning algorithm, the project gains versatility in that the framework can seamlessly be adapted to any machine learning workload simply by propagating that workload to the network for active full nodes to mine. The pavement monitoring machine learning algorithm is inherently suitable for use on this network, the only caveat being the security concerns discussed in the proposal, that need to be addressed prior to user adoption.

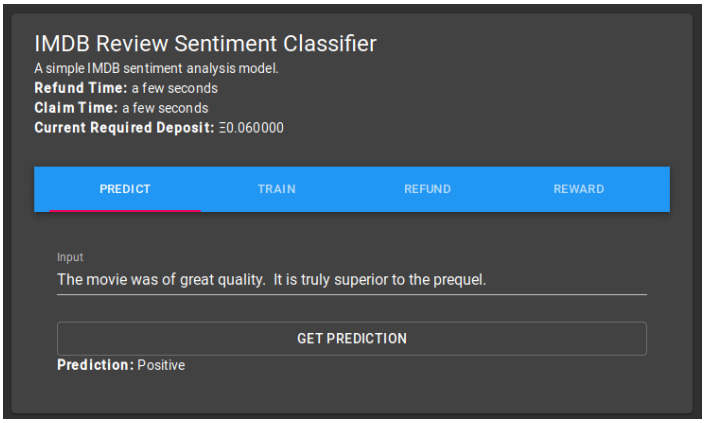

Conclusion

While crowdsensing is a relatively new and unexplored field, it appears to have the potential to solve a myriad of problems. While this project has only made small strides towards a practical application of the concept, the idea of an implementation that bridges the technologies of machine learning and blockchain should not be ignored. With plenty of startups emerging in the intersection of these fields, it is only natural that it should appear under the academic lens. Regardless of the feasibility of a decentralized approach towards the task, the broader avenue of crowdsensing has the prospect of considerable returns on pavement monitoring.

Appendix A - Cross Platform Client App User Manual

1. Take a photo of the road condition, while taking into account lighting and clarity.
2. You will be brought to the upload screen, either hit the Upload button in the bottom right hand corner, or hit Back to retake the photo. The photo is then automatically uploaded to our server for image processing. In the future, this process may be similar, but instead of sending the data to a centralized server, it will be propagated to a network for addition to the blockchain.
3. When the upload is complete, you will be brought to a rewards screen. At the moment, this uses placeholder logic, but will be replaced with accurate representation of the cryptocurrency rewarded based on the contribution.

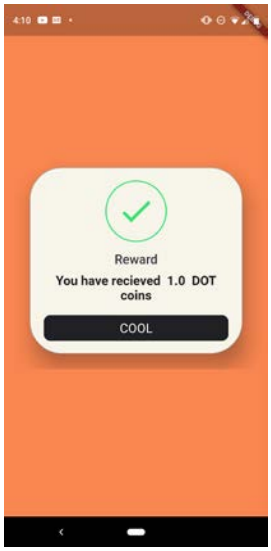

Appendix B - Dashboard App Manual

Enter into the directory of the dashboard app

(i.e cd ~/dotdashboard)

Run the deploy script:

./deploy.sh

Open your browser to “localhost:3000”

This dashboard serves a variety of functions of displaying the data on the centralized server. Much of this is extensible to a model that relies on blockchain technology, so in the future this may look the same but provide different data. Much of this data would involve the visibility of the blockchain, such as the ability to view all transactions on the network, or monitor the total hashing power of all of the participating nodes.

Appendix C - Cross Platform App Developer Manual

1) Install Android Studio https://developer.android.com/studio
2) Install Flutter/Dart https://flutter.dev/docs/get-started/install
3) Install Android Studio Flutter Plugin: File > Settings > Plugins
4) Open “pubspec.yaml” and click “pub get” from the top bar to install all of the dependencies
5) Hit the Run button to deploy the app

Appendix D - Dashboard App Developer Manual

1) Install the following tools:
    a) Node.js/NPM https://www.npmjs.com/get-npm
    b) Yarn https://yarnpkg.com/en/
    c) WebStorm (optional but recommended) or your favorite editor
    d) All project dependencies using “yarn install”, once from within the root project directory, and once within the “server” directory
2) Use “./deploy.sh” to deploy both the dashboard and the middleware

Works Cited

1. “Frequently Asked Questions.” *The American Road & Transportation Builders Association (ARTBA)*, www.artba.org/about/faq/.
2. “Use of Accelerated Pavement Testing to Evaluate Maintenance and Pavement Preservation Treatments.” 2009, doi:10.17226/23000.
3. “A Survey of Mobile Crowdsensing Techniques: A Critical Component for The Internet of Things.” *ACM Transactions on Cyber-Physical Systems*, ACM, dl.acm.org/citation.cfm?id=3185504.
4. Lawson, William D., and Sanjaya Senadheera. “Chip Seal Maintenance.” *Transportation Research Record: Journal of the Transportation Research Board*, vol. 2108, no. 1, 2009, pp. 61–68., doi:10.3141/2108-07.
5. “Pavement Condition Index (PCI).” *FAA PAVEAIR*, faapaveair.faa.gov/Help/PavementConditionIndexPCI.html.
6. Cafiso, S., et al. “From Manual to Automatic Pavement Distress Detection and Classification.” *2017 5th IEEE International Conference on Models and Technologies for Intelligent Transportation Systems (MT-ITS)*, 2017, doi:10.1109/mtits.2017.8005711.
7. Facebook. “Facebook/React-Native.” *GitHub*, 23 July 2019, github.com/facebook/react-native.

8. “JavaScript.” *MDN Web Docs*, developer.mozilla.org/en-US/docs/Web/JavaScript.
9. Chengevelyn. “$24 Million Iced Tea Company Says It's Pivoting to the Blockchain, and Its Stock Jumps 200%.” *CNBC*, CNBC, 26 Dec. 2017, www.cnbc.com/2017/12/21/long-island-iced-tea-micro-cap-adds-blockchain-to-name-and-stock-soars.html.
10. “Laser Crack Measurement System (LMCS).” *Pavemetrics*, www.pavemetrics.com/applications/road-inspection/lcms2-en/.
11. Billström, Adam Hemlin, and Fabian Huss. “Video Integrity through Blockchain Technology - Semantic Scholar.” *Video Integrity through Blockchain Technology - Semantic Scholar*, 2017-08-02, https://www.semanticscholar.org/paper/Video-Integrity-through-Blockchain-Technology-Billström-Huss/6a0e1df59e06ebfe440b38a1bb1ff3b7625fb30a
12. “Ethereum.” *Ethereum.org*, www.ethereum.org/.
13. “Leveraging Blockchain to Make Machine Learning Models More Accessible.” *Microsoft Research*, 19 July 2019, www.microsoft.com/en-us/research/blog/leveraging-blockchain-to-make-machine-learning-models-more-accessible/.